

# Whole-body magnetic resonance imaging for prostate cancer assessment: Current status and future directions

Sandy Van Nieuwenhove, MD,<sup>1</sup> Julien Van Damme, MD,<sup>2</sup> Anwar R. Padhani, MD,<sup>3</sup>   
 Vincent Vandecaveye, MD, PhD,<sup>4</sup> Bertrand Tombal, MD, PhD,<sup>2</sup> Joris Wuts, MSc,<sup>1,5</sup>  
 Vassiliki Pasoglou, MD, PhD,<sup>1</sup> and Frederic E. Lecouvet, MD, PhD<sup>1\*</sup> 

## Abstract

Over the past decade, updated definitions for the different stages of prostate cancer and risk for distant disease, along with the advent of new therapies, have remarkably changed the management of patients. The two expectations from imaging are accurate staging and appropriate assessment of disease response to therapies. Modern, next-generation imaging (NGI) modalities, including whole-body magnetic resonance imaging (WB-MRI) and nuclear medicine (most often prostate-specific membrane antigen [PSMA] positron emission tomography [PET]/computed tomography [CT]) bring added value to these imaging tasks. WB-MRI has proven its superiority over bone scintigraphy (BS) and CT for the detection of distant metastasis, also providing reliable evaluations of disease response to treatment. Comparison of the effectiveness of WB-MRI and molecular nuclear imaging techniques with regard to indications and the definition of their respective/complementary roles in clinical practice is ongoing. This paper illustrates the evolution of WB-MRI imaging protocols, defines the current state-of-the art, and highlights the latest developments and future challenges. The paper presents and discusses WB-MRI indications in the care pathway of men with prostate cancer in specific key situations: response assessment of metastatic disease, “all in one” cancer staging, and oligometastatic disease.

J. MAGN. RESON. IMAGING 2022;55:653–680.

## INTRODUCTION

Prostate cancer (PCa)<sup>1</sup> is the second most common cancer in men, with an estimated 1,276,106 new cases worldwide in 2018.<sup>2</sup> Despite improvement in therapy, PCa remains the fifth leading cause of cancer-related death and is responsible for 3.8% of total cancer deaths.<sup>2</sup>

Patients with newly diagnosed (ND) PCa are stratified into different risk groups based on their clinical state, International Society of Urological Pathology (ISUP) grading, and prostate-specific antigen (PSA) levels in order to define their prognosis and further care.<sup>3</sup> Early detection of high-risk

recurrent cancer after definitive initial therapy is critical because salvage treatments can be successful. Later on, reliable quantification of metastatic burden and monitoring response to therapy are key expectations for imaging.

Next-generation imaging (NGI) techniques such as whole-body magnetic resonance imaging (WB-MRI) and prostate-specific membrane antigen (PSMA) positron emission tomography (PET)/computed tomography (CT) address the clinical need for better stratification of PCa states.<sup>4–6</sup> These techniques are being evaluated for the assessment of local and distant metastasis at the time of initial staging, when

View this article online at [wileyonlinelibrary.com](http://wileyonlinelibrary.com). DOI: 10.1002/jmri.27485

Received Oct 7, 2020, Accepted for publication Dec 8, 2020.

### \*Correspondence

Frederic E. Lecouvet, Department of Radiology, Institut de Recherche Expérimentale et Clinique, Cliniques Universitaires Saint-Luc, Université Catholique de Louvain, Brussels B-1200, Belgium.

Email: [frederic.lecouvet@uclouvain.be](mailto:frederic.lecouvet@uclouvain.be)

Sandy Van Nieuwenhove and Julien Van Damme are first equivalent authors.

From the <sup>1</sup>Department of Radiology and Medical Imaging, Cliniques Universitaires Saint-Luc, Institut de Recherche Expérimentale et Clinique, Université Catholique de Louvain, Brussels, Belgium; <sup>2</sup>Department of Urology, Cliniques Universitaires Saint-Luc, Brussels, Belgium; <sup>3</sup>Mount Vernon Cancer Centre, Mount Vernon Hospital, London, UK; <sup>4</sup>Department of Radiology and Pathology, University Hospitals Leuven, Leuven, Belgium; and <sup>5</sup>Department of Electronics and Informatics (ETRO), Vrije Universiteit Brussel, Brussels, Belgium

biochemical recurrence (BCR) occurs, and in the follow up of men with metastatic disease.

Although there is compelling evidence that WB-MRI and PSMA PET/CT are superior to conventional imaging with bone scintigraphy (BS) and CT for determining disease volume and extent, NCI techniques are still not routinely recommended by international guidelines at the time of first diagnosis even in men with locally advanced PCa.<sup>7-9</sup> Still, NCI techniques are increasingly recognized to have the potential to play an important role in select patients, and PSMA-PET/CT, due to the strength of the evidence, is already recommended in guidelines for BCR patients.<sup>10,11</sup> Even so, the availability of PSMA-PET/CT remains limited, and while awaiting its wider availability, WB-MRI has been proposed as a viable alternative because it does not require a separate, extensive supportive radionuclide production infrastructure, and it provides reliable information for decision-making.

WB-MRI protocols are constantly evolving in order to reliably detect every single lesion, with more time-efficient acquisitions and workflows, so that the necessary information is obtained for clinical decision-making. Anatomical and diffusion sequences have been improved, and several quantitative parameters, for example, apparent diffusion coefficient (ADC; unit  $\text{mm}^2/\text{s}$ ) values and fat fraction (FF; %), bring objectivity to the measurements. Recommendations regarding the choice of sequences and technique, as well as the reading and reporting of images, have emerged.<sup>12,13</sup>

In this paper, we review the design of WB-MRI protocols and their evolution, discuss their clinical roles in the staging and therapeutic pathway of PCa patients, assess their place and limitations compared to other NCI methods, and address future and challenging directions.

## WB-MRI TECHNIQUE: EVOLUTION OF HARDWARE AND SOFTWARE

WB-MRI consists of the acquisition of consecutive stacks of high spatial resolution images of consecutive parts of the body that are then fused using reconstruction software. Initially, WB-MRIs were limited by the need to reposition the patient between each station along with long acquisition times per station, but the introduction of rolling bed platforms and the acceleration of sequences eliminated the need for repositioning and made it possible to scan patients in less than 1 h.<sup>14-16</sup> Advances in radiofrequency coils led to changes from built-in body coils, first used to increase *z*-axis coverage, to whole-body surface coils that combine numerous integrated coil elements, which improved contrast-to-noise-ratio (CNR) and spatial image resolution.<sup>17,18</sup> Today, a continuous increase in the number of receiving channels and improvements in the design and weight of surface coils are increasing the overall performance, resolution, and rapidity of WB-MRI examinations.<sup>18</sup>

Advances in software and acceleration techniques such as parallel imaging technique have enabled faster acquisition of images and have contributed to the emergence of functional techniques such as diffusion-weighted imaging (DWI) using single-shot spin echo planar imaging (ssEPI)<sup>19,20</sup> and quantitative fat imaging using gradient echo-based Dixon approaches. In addition, the growing use of 3T magnets in clinical practice has led to increases in signal-to-noise ratios (SNR) and faster acquisition times and has made acquisition of three-dimensional (3D) isotropic T1 sequences possible.<sup>21,22</sup> Nevertheless, performing 3T WB-MRI is more prone to artifacts and is more challenging.<sup>23</sup>

## TARGET ORGANS: FROM BONE TO ALL-ORGAN IMAGING

In general, the setup of MRI protocols depends on the likely distribution of metastases, which in turn depends on the primary cancer location, stage, and histotype. In PCa, metastatic disease is initially observed in the skeleton and the lymph nodes; visceral locations are less common.<sup>24-26</sup> However, increasingly effective therapies have resulted in an increased incidence of multiorgan metastases during later stages of disease,<sup>27</sup> and an autopsy study of 1589 patients revealed that hematogenous metastases were present in 35% of the patients, and these metastases were located in the skeleton in 90%, the lung in 46% (pleura 21%), the liver in 25%, and the adrenals in 13%.<sup>28</sup> This requires imaging protocols that are able to depict metastases at a variety of anatomic sites during a single examination.

## WB-MRI ANATOMICAL IMAGES

### *From Axial Skeleton to Whole-Body and All-Organ Screening*

Axial skeleton (spine and pelvis) MRI (AS-MRI) combining T1- and short inversion time inversion recovery (STIR)-weighted images of the spine in the sagittal plane, often complemented with coronal images of the bony pelvis, were initially used to study skeletal red bone marrow areas most likely to harbor bone metastases.<sup>29,30</sup> The presence of lesions, epidural extension, and spinal cord compression is assessable.<sup>31</sup> The AS-MRI technique alone was very competitive with BS, although this technique could not detect appendicular, sternal, or rib lesions, but involvement of these sites alone is exceptional.<sup>32,33</sup> The assessment of the spine still remains necessary to complement other WB-MRI sequences in modern practice.

The availability of WB-MRI anatomic sequences made coverage of the whole skeleton in the coronal or axial plane possible, although in practice, this is limited to the region from the eyes to the mid-thighs; more distal limb metastases are exceptional.<sup>33-35</sup> Compared to AS-MRI for the detection of bone lesion, coronal WB-MRI did not detect significantly

more bone metastases (134 with WB-MRI vs. 124 with AS-MRI) in 60 patients.<sup>33</sup> With the introduction of dedicated sequences, for example, breath-hold 3D T1 gradient echo (GRE), WB-MRI protocols evolved to encompass all organs and now enable more complete staging evaluations, which include assessments of lymph nodes, lung and liver parenchyma, and the prostatic bed.<sup>12,36,37</sup>

Initially, WB-MRI protocols relied exclusively on anatomical sequences such as T1 and T2 with fat suppression or STIR-weighted images, sequences that enable the detection of bone metastases. Compared to the normal bone marrow, bone metastases exhibit low signal intensity (SI) on T1-weighted images, and an intermediate to high SI lesion is observed on T2-weighted images, depending on the mineralization status and water content of lesions, and sometimes with a peripheral “cellular” high SI T2 halo thought to reflect more active or aggressive disease surrounding a more mineralized central portion of the lesion.<sup>38</sup>

T2-weighted sequences have been optimized to improve lesion detection by increasing contrast between lesions and the surrounding normal marrow using different methods to suppress the fat signal, that is, chemical shift selective saturation (CHESS), STIR, or the Dixon method (see below).<sup>29,39</sup> These anatomical MRI sequences are sufficient to distinguish bone metastasis from the normal fatty bone marrow background in the majority of patients. Difficulties may be encountered in patients with more cellular marrow, such as in younger individuals and patients being administered bone marrow-stimulating factors, due to the reduced contrast between lesions and the background hyperplastic marrow.<sup>40</sup>

As with CT scans, anatomical WB-MRI sequences also have limited diagnostic value for detecting pathological lymph nodes because the main criterion of metastatic lymph node involvement is based on its size. Anatomic images have low sensitivity and specificity in detecting the microscopic infiltration of normal-sized nodes, a common phenomenon in PCa.<sup>41</sup>

As already noted, visceral metastases mainly affect the liver and lungs and occur at later stages of the disease.<sup>42</sup> WB-MRI anatomical images are progressively being optimized for detecting lung metastases, but there is little objective information concerning their use in the literature.<sup>12</sup> Liver metastases can be efficiently detected using DWI, and characterization of lesions can be carried out using anatomic signal characteristics using DWI (see below) and contrast-enhancement (if necessary).<sup>36,43</sup>

### **From 2D to 3D Imaging: Multiplanar Capability and Speed**

Anatomic images acquired using two-dimensional (2D) sequences are obtained in the coronal or axial plane for skeletal and node screening but also in the sagittal plane for optimal study of the spine. Advances in both hardware and

software have made it possible to obtain 3D images, which allow multiplanar reformatting after acquisition of a single-volume sequence. Initial approaches involved acquiring coronal 3D-T1 fast spin echo (FSE); Sampling Perfection with Application optimized Contrasts using different flip angle Evolution (SPACE); or cube sequences using very thin, nearly isotropic voxels (section thickness of 1.2 mm). These approaches facilitated the detection of bone and node metastases, especially in difficult-to-evaluate anatomic areas (e.g., posterior vertebral elements, pelvic nodes, etc.), and avoided the need for acquiring additional dedicated images of the spine and retroperitoneal lymph nodes<sup>22</sup> (Figure 1), hence saving time. However, a remaining drawback of 3D FSE sequences was an acquisition time of more than 4 min for each station and more than 12 min for whole-body coverage, and the Dixon approach can address this limitation.

### **Contribution of the Dixon Technique to WB-MRI**

The Dixon technique obtains images using two (two-point Dixon) or more (multipoint Dixon, mDixon) echoes.<sup>44</sup> Fat suppression takes advantage of the fact that the nuclei in water and fat molecules precess at different frequencies, alternating over time to being in-phase (IP) and out-of-phase/opposed-phase (OP) with each other. The Dixon technique enables the reconstruction of four types of images: IP and OP images but also fat-only (FO) and water-only images (WO, which correspond to fat-saturated images).

Breath-hold 3D-T1 GRE images acquired using the Dixon technique can decrease the acquisition time for anatomical images. The value of one pelvic 3D T1-weighted GRE sequence with a 2-point Dixon fat–water separation was compared to T1W FSE in 39 PCa patients. The sequence provided better image quality, equivalent performance for node and bone detection, and a reduced acquisition time (2 min 37 s vs. 5 min 16 s).<sup>45</sup> The Dixon technique was first introduced in WB-MRI for bone lesion screening in metastatic breast cancer<sup>46–48</sup> and in myeloma<sup>49</sup> in association with DWI sequences. The FO images improved contrast between tumoral lesions and the normal marrow, which is sometimes limited on T1 IP images.<sup>50</sup> A WB-MRI study compared the performance of the 3D T1 GRE breath-hold mDixon sequence to 3D T1-FSE for the detection of node and bone metastases in 30 patients with high-risk PCa and demonstrated that the accuracy of 3D mDixon T1 GRE was comparable to 3D T1 FSE, while acquisition times were shortened significantly from 14 min to 1 min 20 s.<sup>51</sup> The T1 GRE mDixon technique has also been assessed for node and bone metastases screening in PCa and was found to perform better than BS for detecting bone metastases and similar to <sup>18</sup>F choline-PET/CT for detecting malignant node involvement.<sup>52</sup> The Dixon acquisition also showed promise for detecting lung metastases and exhibited a similar performance to low-dose CT on a per-patient basis. Of note, ultra-short



**Figure 1:** Comprehensive whole-body magnetic resonance imaging (WB-MRI) used for staging of newly diagnosed prostate cancer in a 74-year-old man at high risk of metastasis. (a) Coronal 3D T1-weighted (W) turbo-spin echo (TSE) sequence shows a unique left femoral neck metastasis (arrow). (b) Coronal reformatted DWIBS image at  $b$  1000  $s/mm^2$  diffusion DWI (multiplanar reconstruction, inverted grayscale) confirms left femoral neck lesion (arrow). Note that the dark signal of the brain, spleen, and spinal cord and small lymph nodes in the neck, axillae, and groin are a normal finding. (c) Sagittal reformatted 3D T1W FSE image of the spine show no vertebral metastasis. (d) Transverse reformatted 3D T1W TSE image confirms the presence of a left femoral neck metastasis. (e) Fat fraction (F%) map obtained using the Dixon technique shows complete disappearance of fat pixels within the metastatic deposits. (f) ADC map shows abnormal signal within the femoral lesion ( $1235 \mu m^2/s$ ). F% and ADC values may be used for lesion monitoring

echo time (UTE) acquisitions can also be used to assess lung parenchyma as UTE can detect pulmonary nodules that are 5 mm or larger, but this adds significantly to scan time.<sup>53</sup> Conventional Dixon MR images are less able to detect nodules smaller than 10 mm.<sup>54–56</sup> Recent advances include breath-hold lung sequences, which promise shorter acquisition times while maintaining lesion detection sensitivity of lesions sized 5 mm or more; these sequences require further evaluations.

### Fat Fraction Measurements

Dixon acquisitions can be used to generate fat fraction maps.<sup>57</sup> The signal or relative fat fraction (sFF/rFF; unit %) is calculated using the formula:  $(SI_{FO}/[SI_{FO} + SI_{WO}]) \times 100$ . The calculated sFF value is reproducible with a small standard deviation for repeated measurements ( $\sigma R = 13\%–32\%$ ).<sup>58,59</sup> sFF maps provide a quantitative assessment of bone marrow fat and can be used to assess treatment response.<sup>58,60–62</sup> A retrospective comparison of sFF and ADC values of 43 bone lesions with histology showed that active bone lesions had a significantly lower sFF (11.5% vs. 62%) and median ADC ( $898 \times 10^{-6}$

vs.  $1617 \times 10^{-6} mm^2/s$ ) compared to responding lesions<sup>63</sup> (Figure 1).

### T2-Dixon: Tomorrow's Single Anatomic Sequence?

According to guidelines, whole-spine sagittal fat-suppressed T2 or STIR images are recommended in WB-MRI protocols to study vertebral lesions and their complications.<sup>12</sup> The added value of the T2 Dixon method is notable because it provides a more uniform suppression of the fat signal and higher SNR and CNR, making bone lesions more conspicuous compared to other techniques, including CHES or STIR sequences.<sup>46–48</sup> In one sequence, the T2 Dixon technique offers improved sensitivity emanating from WO images (equivalent to T2 fat-saturated or STIR images); the effectiveness of T2 IP images for the study of the spinal canal, discs, and marrow; the ability to evaluate lymph nodes; and the “T1-like” information of FO/FF images, which provide high contrast between bone metastases and normal marrow.

In the spine, a retrospective analysis compared whole-spine sagittal T2 mDixon FSE to T1 FSE in 121 patients with metastatic involvement and found an equivalent

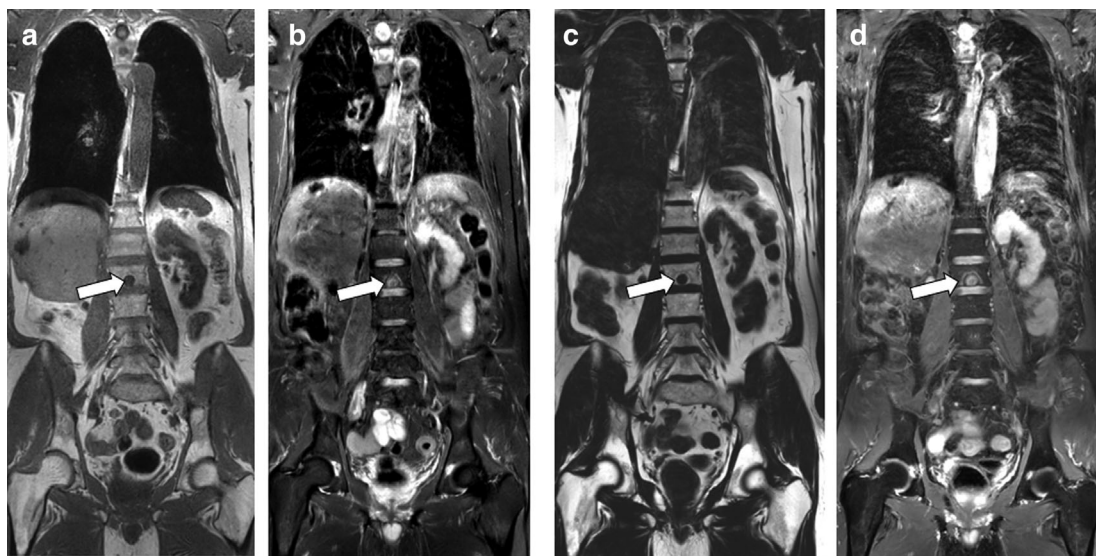


**Figure 2:** Value of a single T2 Dixon sequence as alternative to the combination of T1 and STIR sequences as anatomical sequences. Staging in 55-year-old man with ND prostate cancer (PCa) at high risk of metastasis. (a, b) Coronal T1 TSE and STIR images show a metastasis within the L2 vertebral body (arrow). (c, d) Fat only (c) and Water only (d) images obtained from one single T2 Dixon TSE acquisition show the same lesion (arrows)

performance between the FO images derived from the T2 Dixon acquisition and the T1 images.<sup>64</sup> Furthermore, T2 mDixon had better CNR (181 vs. 84.7) and good to very good interobserver agreement. Another retrospective study compared the performance of sagittal mDixon T2-TSE to the conventional T1-TSE images in 33 patients with 68 metastases and also found no differences between FO images from the T2 Dixon acquisition and T1 sequence.<sup>65</sup> The acquisition time of the T2 Dixon sequence is longer (6 min 15 s vs. 4 min 14 s for the T1 sequence), but, overall, the Dixon approach provides both FO (T1-like) and WO (STIR-like) images in shorter times than the guideline-recommended combination of T1 and STIR images. Using T2 Dixon sequences as an alternative to the sum of T1 and STIR for WB-MRI anatomical sequences images could drastically shorten the acquisition times, but this remains to be evaluated in comparative studies (Figure 2).

Both T2- and T1-weighted sequences acquired using the Dixon method can be affected by the fat–water swapping artifacts, especially in heterogeneous anatomic regions (neck, close to metallic implants), leading to the replacement of a part of the fat-only image by part of the water-only image and vice versa. This artifact is quite easy to identify, and the reading must then be made by side-by-side analysis of FO and WO images.<sup>66,67</sup>

## FUNCTIONAL MRI: DWI

### Standard DWI

The introduction of whole-body DWI with background body signal suppression (DWIBS) using STIR–echo-planar imaging sequence (STIR EPI) during free breathing

allowed acquisition of whole-body DWI with reduced slice thickness and homogeneous fat suppression.<sup>29,30,33,34,68–72</sup> Fat-suppressed (most frequently using the inversion recovery technique) DWI sequences using high-diffusion sensitizing gradients (b-values; unit  $s/mm^2$ ) are generally acquired in the axial plane from head to mid-thigh. For DWIBS, STIR is preferred over CHES for more uniform fat suppression because of its lower sensitivity to magnetic field inhomogeneities, and images are acquired using free breathing.<sup>72</sup> Two or more b-values are acquired, and ADC maps are calculated with monoexponential fitting of the signal intensity data. A lower b-value in the range 50–100  $s/mm^2$  minimizes the contribution of microcirculation perfusion effects. A higher b-value set between 800 and 1000  $s/mm^2$  attenuates the SI of normal tissues without compromising SNR.<sup>73</sup> Intermediate b-values of 500–600  $s/mm^2$  may be considered to improve the accuracy of calculated ADC maps.<sup>12</sup>

DWI sequences are usually read on Picture Archiving and Communication System (PACS) workstations using multiplanar reformatting (MPR) and maximal intensity projection (MIP). Both lower and high b-value images should be evaluated synchronously with the anatomical images.<sup>12</sup> Reconstructed high b-values DWI images allow the visualization and measurement of focal lesions on native or inverted grayscale contrast, usually displayed as multiplanar reformatted views or MIPs.

Before interpreting WB-DWI images, the reader should be familiar with the normal appearance of the bone marrow and lymph nodes. Normal yellow bone marrow in adults has low perfusion and is mainly composed of large fat cells, which impede the movement of extracellular water molecules,

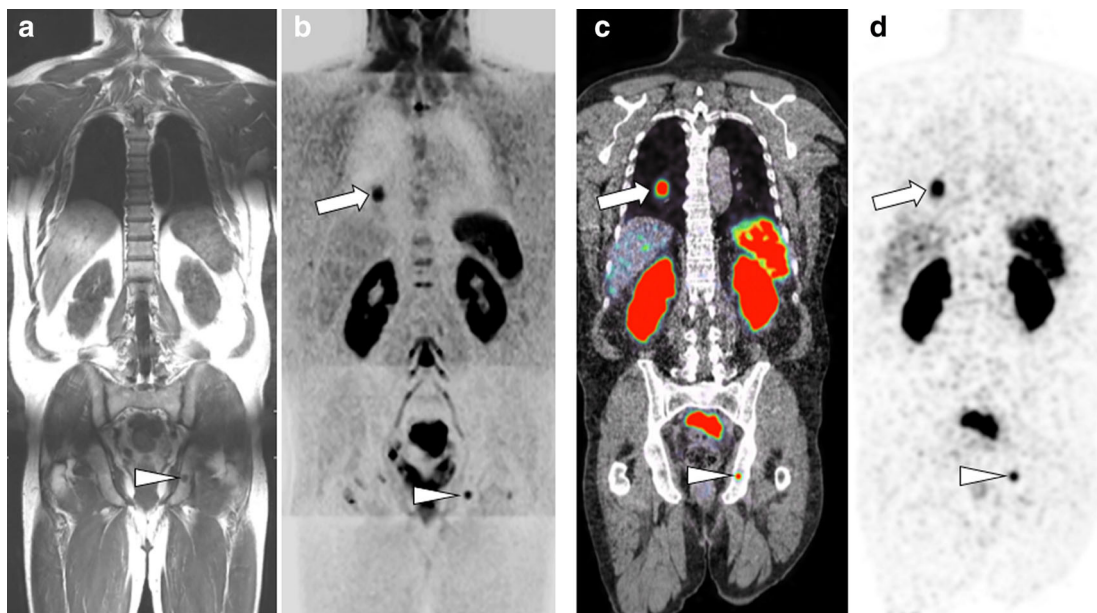


**Figure 3:** Whole-body magnetic resonance imaging (WB-MRI) and  $^{64}\text{Ga}$ -PSMA PET/CT obtained in the same week in a 63-year-old man with advanced prostate cancer (PCa). (a, b) Coronal WB-MRI (a) T1 TSE and (b) coronal reformatted DWIBS (b 1000; inverted grayscale) images show right lung (arrow) and left ischiopubic bone (arrowhead) metastasis. (c, d)  $^{64}\text{Ga}$ -PSMA-PET/CT: reformatted fused PET/CT (c) and metabolic PET (d) images show the same lung (arrow) and bone metastasis (arrowhead)

causing a low SI in high b-value images and low ADC values.<sup>74</sup> Normal red bone marrow has a higher perfusion, cellularity, and water content, which results in higher SI in high b-value images and higher ADC values. Of note, false-positive observations due to high SI on high-b-value images include the T2 shine-through effect from benign vertebral lesions (e.g., hemangioma, endplate degenerative changes), but these pitfalls can be easily overcome by correlating high b-values images to anatomical sequences and corresponding ADC values.<sup>75</sup>

Normal ADC values of adult bone marrow range from  $0.2 \times 10^{-3} \text{ mm}^2/\text{s}$  to  $0.6 \times 10^{-3} \text{ mm}^2/\text{s}$ .<sup>20</sup> ADC values of bone marrow decrease with aging in proportion to an increase in fat content accompanying osteoporosis and age-related marrow atrophy.<sup>76,77</sup> Bone metastatic disease appears as focal or diffuse areas of increased SI on high b-value images and higher ADC compared to normal bone marrow. Tumor ADC values have an upper range value of  $1.2\text{--}1.4 \times 10^{-3} \text{ mm}^2/\text{s}$ . An ADC threshold of  $0.655 \times 10^{-3} \text{ mm}^2/\text{s}$  was shown to separate normal bone marrow in healthy volunteers from abnormal bone marrow in 23 PCa, 9 breast cancer, and 11 myeloma patients.<sup>78</sup>

The presence of bone edema, increased cellularity from bone marrow stimulation, or focal bone marrow hyperplasia may be responsible for increased marrow signal and should not be misinterpreted as a diffuse or progression disease.<sup>73</sup> False-negative DWI results may be encountered in hypercellular bone marrow due to reduced contrast between metastases and the marrow background,<sup>73</sup> in densely sclerotic bone lesions,<sup>79</sup> and in some difficult anatomical areas such as the lower neck and ribs.

The detection of abnormal lymph nodes remains difficult with DWI. Both normal and pathological nodes have high SI in high-b value images because of their high cellularity. Hence, similar to anatomic images, size remains the main diagnostic criterion for abnormal nodes. ADC measurements have been proposed to improve the value of DWI sequences to distinguish malignant from benign lymph nodes presenting a “normal” size. Malignant nodes have been shown to have significantly lower ADC values ( $1.07 \pm 0.23 \times 10^{-3} \text{ mm}^2/\text{s}$ ) than benign nodes ( $1.54 \pm 0.25 \times 10^{-3} \text{ mm}^2/\text{s}$ ) in several studies.<sup>80–82</sup> Studies have also found lower but nonsignificant ADC values in metastatic lymph nodes ( $0.92 \pm 0.22$  and  $0.94 \pm 0.18 \times 10^{-3} \text{ mm}^2/\text{s}$ ) than in benign nodes ( $1.04 \pm 0.18$  and  $1.01 \pm 0.28 \times 10^{-3} \text{ mm}^2/\text{s}$ ).<sup>83,84</sup>

As for visceral metastases, pulmonary nodules and liver lesions may be detected as focal high-signal lesions on high b-value images (Figure 3). A study including 22 patients (17 with PCa) demonstrated a high sensitivity (96%) of WB-MRI for the detection of visceral metastases compared to CT,  $^{18}\text{F}$  fluorodeoxyglucose (FDG) PET/CT, and  $^{11}\text{C}$  choline acetate PET/CT<sup>85</sup> (Figure 4).

### Computed DWI and Semiautomatic Segmentation

Computed WB-DWI consists of generating postprocessed images at user-defined higher b-values based on voxel MR signal and ADC values.<sup>86</sup> The generated images can help reduce the T2 shine-through effect on MIP images; reduce near-field flare signal, especially on images acquired at 3T; and can facilitate semiautomatic segmentation on MIP WB-DWI with better delineation of the tumor volumetric burden (total

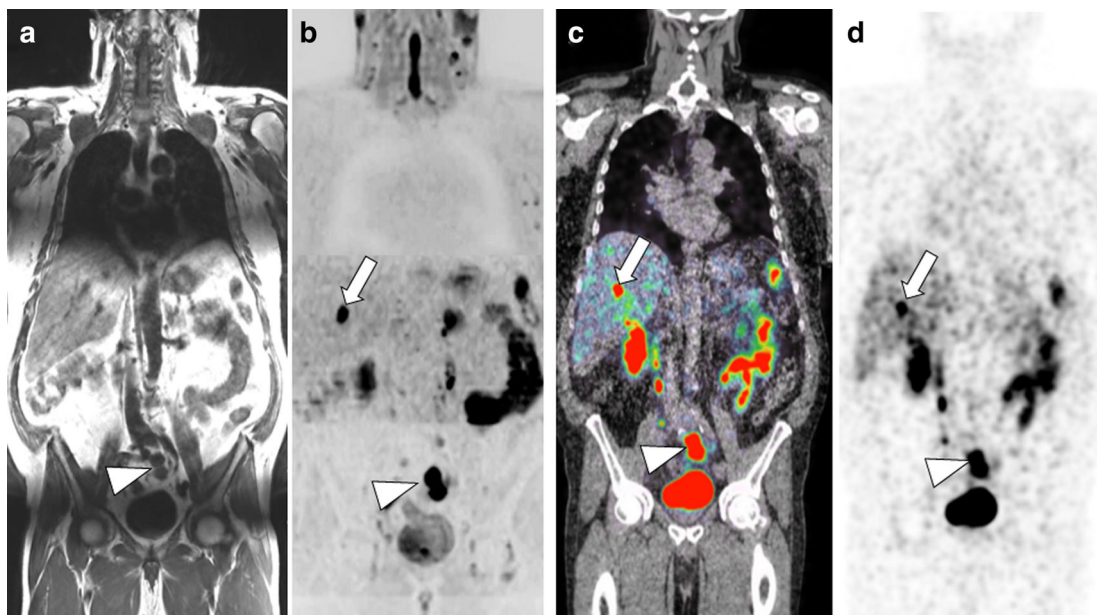


**Figure 4:** Whole-body magnetic resonance imaging (WB-MRI) and PSMA PET/CT obtained in the same week in a 68-year-old man with advanced prostate cancer (PCa). (a, b) Coronal WB-MRI (a) T1 TSE and (b) coronal reformatted DWIBS (b 1000; inverted grayscale) images show liver metastasis (arrow) and common iliac metastatic lymph nodes (arrowhead). (c, d)  $^{68}\text{Ga}$ -PSMA-PET/CT: reformatted fused PET/CT (c) and metabolic PET (d) images show the same lung (arrow) and bone metastasis (arrowhead)

Diffusion Volume, tDV).<sup>87</sup> However, their routine use is not recommended.

### Simultaneous MultiSlice-DWI

Simultaneous excitation and acquisition of multiple slices allows an acceleration of data acquisition with a limited impact on SNR.<sup>88</sup> Parallel imaging and the CAIPIRINHA technique (controlled aliasing in parallel imaging results in higher acceleration) permit the potential use of simultaneous multislice (SMS)-DWI in whole-body DWI.<sup>89</sup> Using PET/MRI, a study compared SMS-DWI to DWIBS in 10 volunteers and 20 patients at 3 T.<sup>90</sup> Acquisition time was reduced by 40% (84 s vs. 140 s) with a subjective cost in image quality and more artifacts observed in the thoracoabdominal area of the SMS-DWI images. Still, SMS-DWI provided reliable lesion conspicuity, and the ADC values were reliable and comparable to standard DWI. Whole-body SMS-DWI was recently used for bone metastases screening in PCa and showed similar image quality compared to standard DWI.<sup>91</sup> Deep learning methods for image reconstruction are also emerging, which will further reduce DWI sequence acquisition times. These methods are still not widely available, and their impact on WB-MRI use cannot yet be evaluated.

### MULTIPARAMETRIC WB-MRI AND CHOICE OF SEQUENCES

Multiparametric (mp) MRI, the association of anatomical and at least two functional sequences, represents the current standard for studies dealing with the local assessment of

prostate,<sup>92</sup> breast,<sup>93</sup> bladder,<sup>94</sup> and brain<sup>95</sup> cancers. WB-MRI provides the same qualitative and quantitative mp approach, relying on anatomical T1 and STIR sequences and functional DWI sequences, along with ADC maps and FF maps for the quantitative evaluation of bone lesions.

In 2016, an international expert panel designed the METastasis Reporting and Data System for prostate cancer (MET-RADS-P) in an attempt to harmonize and standardize WB-MRI protocols in terms of content, quality, and reporting. The core protocol comprises anatomical sequences, including sagittal T1 and T2 fat-suppressed or STIR images of the spine and coronal or axial whole-body T1 GRE Dixon images along with FF mapping (Table 1). The 3D T1 FSE was proposed as the single alternative to the previous T1 sequences. Axial WB-DWI with two b-values (b 50–100 and b 800–1000  $s/\text{mm}^2$ ) is also part of this protocol (Figure 1). MET-RADS-P also proposed a more comprehensive protocol with coronal and axial T1 GRE, axial FSE T2-weighted sequences for node and visceral screening, a higher number of b-values for the WB-MRI sequence, and optional contrast-enhanced sequences. MET-RADS-P also provided response evaluation criteria for bone, node, and visceral lesions.<sup>12</sup>

The United Kingdom Quantitative WB-DWI Technical Workgroup addressed the question of harmonization of quantitative DWI in order to optimize the response assessment of bone metastases, and they proposed that the calculation of ADC be based on two b-values, b = 50–100  $s/\text{mm}^2$  and b = 800–1000  $s/\text{mm}^2$ .<sup>29</sup>

A recent study compared the diagnostic accuracy of the individual T1, STIR, and DWI sequences and their various

**Table 1. Proposed whole-body magnetic resonance imaging (WB-MRI) sequences and acquisition parameters at 3T (modified according to METastasis Reporting and Data System for prostate cancer (MET-RADS-P)<sup>12</sup>)**

Sequence type	T1 GRE DIXON	Spine T1 TSE	3D T1 TSE <sup>a</sup> (alternative)	Spine T2 STIR	T2 TSE DIXON <sup>b</sup> (alternative)	T2 TSE <sup>c</sup>	DWI (DWIBS)
Imaging plane	Coronal and/or axial <sup>c</sup>	Sagittal	Coronal	Sagittal	Sagittal	Axial	Axial
Fat suppression	—	—	—	STIR	—	—	STIR
Respiratory control	Breath-hold	Free breathing	Free breathing	Free breathing	Free breathing	Breath-hold	Free breathing
TR, TE (ms)	3.8/1.46,2.6	555/10	285/21	4714/50	4340/88	562/80	6000/66
FOV (mm)	300 × 450	360 × 360	500 × 299	360 × 360	260 × 349	400 × 300	440 × 348
Slice thickness /Gap (mm)	3 mm/0	3.5/0.35	1.2/0	3.5/0.35	3.5/0.35	4/0	6/0.1
Matrix	300 × 200	260 × 285	320 × 320	320 × 256	260 × 285	308 × 186	128 × 96
Voxel size (mm <sup>3</sup> )	1.5 × 1.5 × 3	0.8 × 1 × 3.5	1.14 × 1.13 × 1.2	0.8 × 1 × 3.5	0.8 × 1 × 3.5	1.3 × 1.6 × 4	4.5 × 4.5 × 6
Diffusion b-value (s/mm <sup>2</sup> )	—	—	—	—	—	—	50/800
Functional map	Fat fraction	—	—	—	—	—	50/500/800 <sup>c</sup>
TA per station (min, s)	0 min 19 s	4 min 20 s	4 min 36 s	3 min 32 s	4 min 24 s	0 min 20 s	3 min 06 s

Abbreviations: 3D, three-dimensional; ADC, apparent diffusion coefficient; DWI, diffusion-weighted imaging; DWIBS, diffusion-weighted whole-body imaging with background body signal suppression; GRE, gradient echo; MET-RADS-P, METastasis Reporting and Data System for Prostate Cancer; STIR, short tau inversion recovery; TA, time acquisition; TSE, turbo spin echo.

<sup>a</sup>3D T1 FSE may replace T1 Dixon and T1 TSE of the spine.

<sup>b</sup>Sagittal T2 Dixon may replace T1 and T2 FSE STIR of the spine.

<sup>c</sup>MET-RADS-P: comprehensive protocol includes both axial and coronal T1 GRE Dixon, axial T2 on the abdomen to detect nodes, and 3b-values in the DWI sequence (additional b 500 s/mm<sup>2</sup>).

combinations (T1-DWI, T1-STIR, STIR-DWI, and T1-STIR-DWI) to detect bone metastases in WB-MRI in 50 patients with PCa and showed that the combination of sequences T1-DWI and T1-STIR was sufficient with no difference in performance using the combination of all three, T1-STIR-DWI, sequences ( $p > 0.07$ ).<sup>96</sup> In practice, however, the combination of T1 and DWI may be preferred as DWI outperforms SNR in detecting node and visceral metastasis (Figures 3 and 4). Moreover, another study found that STIR images did not lend incremental value to WB-MRI coronal T1-weighted images in metastatic screening.<sup>97</sup>

The need for sequences to be used following contrast injection is often questioned. Bone lesions can be differentiated from normal bone marrow (where perfusion is low) with quantitative and semiquantitative parameters on dynamic contrast-enhanced (DCE) images. For example, PCa lesions have been shown to have a significantly higher transfer constant ( $K^{\text{trans}}$ , the permeability surface area product) and high increases in SI and the gradient of the upslope using DCE-MRI sequences.<sup>98</sup> Some investigators have suggested including regional DCE for the detection and characterization of bone metastases, as well as performing a delayed whole-body contrast-enhanced phase in the equilibrium phase at approximately 3 min after contrast medium injection as the contrast medium concentration levels last for about 5.5 min.<sup>99,100</sup> Although recent work suggests that contrast-enhanced 3D T1 GRE sequences represent the most effective sequence along with DWI to detect metastases,<sup>101</sup> contrast-enhanced sequences have limited value for the detection of bone and node lesions and are not included in routine WB-MRI protocols for metastasis<sup>52</sup> or myeloma lesion detection.<sup>102</sup>

## TECHNICAL CHALLENGES

### **Registration and Postprocessing Strategies**

Reconstruction of multistation anatomical and DWI sequences requires postprocessing software that combines the different stacks of images in one volume dataset. WB-MRI is a sum of three to six stacks of high-resolution images that have variations in SI and contain artifacts that are sequence-specific or related to patient motion. In order to overcome these inconsistencies, images acquired for each section are overlapped. Consequently, interscan inhomogeneities at the edge of each section and intrascan inhomogeneities within each stack may be seen,<sup>103</sup> and a variety of methods has been proposed to overcome these inhomogeneities and allow optimal reconstruction.<sup>104</sup> Even so, postprocessing software may fail to provide perfect image alignment and can result in artifacts such as “broken/dancing spine,” with DWI sequences being particularly sensitive to misalignments. Geometrical artifacts can lead to inaccurate assessments of ADC values or lesion sizes. A recently proposed postprocessing, noise-corrected, exponentially weighted DWI (niceDWI) approach

was developed to standardize SI and generate quantitative contrast in WB-MRI studies on PCa.<sup>4</sup> An alternative method consists of using integrated slice-by-slice shimming, which significantly improves the SNR of WB-DWI in the neck region.<sup>105</sup>

### **Artificial Intelligence**

In the future, we can expect the routine use of deep-learning, artificial intelligence (AI) reconstruction techniques to further optimize data acquisition and image reconstructions free of artifacts. Deep learning can reduce the computational time for the reconstruction of parallel imaging and compressed sensing techniques. Indeed, trained deep-learning models optimize the reconstruction process or reduce artifacts in a better assessment of sparsity and sampling of k-space.<sup>106</sup> The diagnostic performance with regard to the reading time of WB-MRI by the radiologist alone or with the assistance of AI is under study.<sup>107</sup>

## CLINICAL INDICATIONS AND POSITIONING OF WB-MRI AMONG OTHER TECHNIQUES

### **Newly Diagnosed Prostate Cancer**

The imaging workup at initial diagnosis must distinguish localized/locally advanced from metastatic PCa and evaluate the metastatic load (Tables 2 and 3). Indeed, patients with localized disease will be treated with local treatment, while those with metastatic disease may benefit from combined systemic and local treatment if they present with fewer than five bone metastases.<sup>1,121</sup> European guidelines recommend at least cross-sectional abdominopelvic imaging (CT or MRI) and a BS for metastatic screening in patients with unfavorable intermediate- and high-risk localized or locally advanced disease, that is, those with a Gleason score of 7 (4 + 3) or a PSA level between 10 and 20 ng/mL (Table 2).<sup>8,9</sup> National Comprehensive Cancer Network (NCCN) guidelines recommend performing abdominopelvic imaging only if nomograms based on clinical features predict >10% probability of pelvic lymph node involvement and performing bone imaging in unfavorable intermediate- and high-risk localized PCa<sup>7,122</sup> (Table 2).

Currently, WB-MRI and PET/CT are not recommended by guidelines for routine use at initial staging, except for equivocal bone lesions on conventional imaging.<sup>11</sup> This is because the clinical benefit of an earlier detection of metastases remains unclear for the whole population.<sup>123</sup> However, it has been abundantly demonstrated that WB-MRI and PET/CT can more accurately define the extent of the disease, locally and remotely, and help tailor a more personalized treatment plan for patients. According to the recent American Society of Clinical Oncology guidelines, however, WB-MRI may be proposed as a second line in high-risk patients with negative/equivocal conventional imaging or in

**Table 2. Current recommendations for imaging workup in localized newly diagnosed prostate cancer (PCa)**

Any risk group staging
Use prebiopsy mpMRI for staging information
Low risk (PSA ≤ 10 ng/mL and ISUP1 and cT1-2a)
No additional imaging is indicated for staging purposes
Intermediate Risk (PSA 10-20 ng/mL or ISUP 2-3 or cT2b)
EAU
In ISUP grade ≥ 3, include at least a cross-sectional abdominopelvic imaging and bone scan for metastatic screening.
NCCN
Bone imaging: only recommended if PSA > 10 ng/mL or T2
Abdominopelvic imaging: recommended if nomogram predicts >10% probability of pelvic lymph node involvement.
AUA
Clinicians should consider staging unfavorable intermediate-risk localized PCa with cross-sectional imaging (CT or MRI) and BS.
High risk (PSA ≥ 20 ng/mL or ISUP 4–5 or ≥ cT2c) or locally advanced (any PSA, any ISUP, cT3-4 or cN+)
EAU
Perform metastatic screening including at least cross-sectional abdominopelvic imaging and bone scan.
NCCN
Bone imaging: recommended.
Abdominopelvic imaging: recommended if nomogram predicts >10% probability of pelvic lymph node involvement.
AUA
Clinicians should stage high-risk localized PCa with cross-sectional imaging (CT or MRI) and BS.
<i>Note:</i> Recommendations based on European Association of Urology, European Society for Radiotherapy and Oncology, and International Society of Geriatric Oncology (EAU-ESTRO-SIOG) guidelines 2020 and National Comprehensive Cancer Network (NCCN) guidelines, version 2.2020. Abbreviations: c, clinical; CT, computed tomography; EAU, European Association of Urology; ISUP, International Society of Urological Pathology; mpMRI, multiparametric magnetic resonance imaging; MRI, magnetic resonance imaging; N, node; NCCN, National Comprehensive Cancer Network; T, tumor.

patients with a few deposits on BS/CT scans that may benefit from additional metastasis-directed therapies (MDT).<sup>124–126</sup> Thus, current guidelines still do not recommend first-line NGI use outside clinical trials.<sup>127,128</sup>

In bones, standard imaging modalities have poor diagnostic accuracy for metastatic staging. CT has a modest pooled sensitivity, 72.9%, and specificity, 94.8%, for detecting bone metastases.<sup>129</sup> Technetium 99 m (<sup>99</sup>Tc) diphosphonate demonstrates up to 40% false-positive results as it detects osteoblastic activity that can be seen in either metastasis but also in benign conditions like inflammation or fractures.<sup>130</sup> Single Photon Emission Computed Tomography (SPECT)–CT can improve the specificity and the positive predictive value of BS, improving

the accuracy of metastatic staging and allow downstaging of metastatic disease in 29.5% of PCa patients.<sup>131</sup> Numerous studies have shown that AS-MRI and WB-MRI outperform BS for bone metastatic screening,<sup>113</sup> and a comparison of WB-MRI with other modalities for newly diagnosed (ND) and BCR of PCa is presented in Table 3 (Panels A and B).

Few studies have investigated the diagnostic performance of <sup>68</sup>Ga-PSMA PET/CT in the assessment of bone metastasis at initial staging,<sup>132</sup> but a recent systematic analysis did conclude that <sup>68</sup>Ga-PSMA PET/CT detects more bone metastases than BS and improves the diagnostic performance for staging ND PCa.<sup>133</sup> In the prospective, multicenter ProPSMA study, the sensitivity and specificity of <sup>68</sup>Ga-PSMA

**Table 3. Comparisons of whole-body magnetic resonance imaging (WB-MRI) to other modalities**

Imaging modality	Study design	Magnetic field strength	Sequences	Reference standard	Patients (n), status (ND, BCR), M (n)	Sensitivity (patient basis)	Specificity (patient basis)
Panel A: Comparisons of WB-MRI to other modalities in ND PCa							
AS-MRI vs. BS +/-TXR <sup>108</sup>	Prospective consecutive enrollment	1.5T	T1/T2W	BVC	66, 26 High risk ND PCa, 28 progression under ADT, 12 BCR, 41 BM	46% BS, 63% BS/TXR, 83% BS/TXR/MRI, 100% MRI	32% BS, 64% BS/TXR, 100% BS/TXR/MRI, 88% MRI
WB-MRI vs. <sup>11</sup> C-Choline PET/CT <sup>109</sup>	Prospective consecutive enrollment	1.5T	T1/STIR/DWI	BVC	11, NR, 11 BM	Not reported, DWI = STIR = <sup>11</sup> C-choline PET/CT	Not reported
AS-MRI vs. BS +/-TXR <sup>30</sup>	Retrospective	1.5 T	T1/T2W	BVC	39 High risk ND PCa, 7 BM	70% BS, 100% MRI	70% BS, 100% MRI
AS-MRI vs. BS <sup>110</sup>	Retrospective	1.5T	T1/STIR	BVC	99, High risk ND PCa, 14 BM	71.4% BS, 85.7% MRI	96.5% BS, 97.7% MRI
WB-MRI vs. BS <sup>111</sup>	Prospective consecutive enrollment	1.5T	DWI	BVC	36 (11 PCa - 3 exclusion/25 BCa), High risk ND PCa, 7 BM (1 PCa/6 BCa)	Patient <5 BM: 58%–67% BS, 33%–58% DWI; Patient>10 BM: BM: 42%–48% BS, 91%–97% DWI	Patient <5 BM: 97% BS, 99% DWI; Patient>10 BM: 97% BS, 99% DWI
WB-MRI vs. 18F-NaF PET/CT <sup>112</sup>	Prospective Consecutive enrollment	1.5T	T1/STIR/DWI	BVC	49, High risk ND PCa, 5 BM	Not reported, MRI = PET/CT	Not reported, 1 FP MRI, 4 FP PET/CT
WB-MRI vs. BS +/-TXR CT (node) <sup>113</sup>	Prospective Consecutive enrollment	1.5T	T1/STIR/DWI	BVC	100, 44 ND High risk PCa, 35 progression under ADT, 21 BCR, 51 BM, 44 NM, 68 B + NM, 13 VM	BM: 86% BS/TXR, 98%–100% MRI, NM: 77%–82% CT, 77–82% MRI, BM + NM: 84% BS/TXR + CT, 91%–94% MRI	BM: 98% BS/TXR, 98%–100% MRI, NM: 95%–96% CT, 96%–98% MRI, BM + NM: 94%–97% BS/TXR + CT, 91%–96% MRI
BS, SPECT, SPECT/CT, <sup>18</sup> F-	Prospective Consecutive enrollment	1.5T	T1/STIR/DWI	BVC	53 (27 PCa/ 26 BCa), High risk ND PCa, 8 BM	79% BS, 89% SPECT, 89% SPECT/CT,	91% BS, 80% SPECT, 94% SPECT/CT,

Table 3. Continued

Imaging modality	Study design	Magnetic field strength	Sequences	Reference standard	Patients (n), status (ND, BCR), M (n)	Sensitivity (patient basis)	Specificity (patient basis)
NaF, PET/CT, WB-MRI <sup>114</sup>						95% PET/CT, 100% MRI	97% PET/CT, 97% MRI
WB-MRI vs. BS <sup>18</sup> F-choline PET/CT <sup>52</sup>	Prospective Consecutive enrollment	3T	mDIXON pre- and post-contrast/T2W/DWI	BVC	56, 6 Intermediate/50 high ND risk PCa, 10 BM, 8 NM	NM:100% MRI, 100% PET/CT, BM: 90% MRI, 80% PET/CT, 60% BS	NM: 96% MRI, 82% PET/CT, BM: 88% MRI, 92% PET/CT, 100% BS
BS, CT, SPECT-CT, <sup>18</sup> F-PSMA-1007 PET/CT, WB-MRI <sup>115</sup>	Prospective Consecutive enrollment	1.5T	Axial T2 FS HASTE, BVC STIR DWI, coronal T1 3D VIBE Dixon, sagittal T1, T2 STIR TSE of spine	BVC	80 High risk ND PCa (1 exclusion)	33%–57% CT, 33%–67% SPECT-CT, 43%–67% WB-MRI, 86%–95% PSMA PET/CT	33%–98% CT, 74%–98% SPECT-CT, 80%–96% WB-MRI, 76%–90% PSMA PET/CT
Panel B: Comparisons of WB-MRI to other modalities at BCR in PCa							
<sup>18</sup> F-choline PET/CT vs. AS-MRI <sup>116</sup>	Prospective Consecutive enrollment	Not reported	T1/STIR/T2FS	BVC	64, BCR postlocal treatment, 15 BCR (BM)	BR: 87% PET/CT, 100% MRI	BR: 96% PET/CT, 100% MRI
<sup>11</sup> C-choline PET/CT vs. WB PET/MRI <sup>117</sup>	Prospective Consecutive enrollment	3T	3D-T1 VIBE/T1W/ T2 HASTE + Axial T2/DWI/DCE pelvis	BVC Histology (n = 19)	75, BCR post-RP (57), RT (14), ADT (4), 37 BCR (37 LR, 37NR, 14BR)	Not reported, Detection rate 84.7% PET/MRI, 77.3% PET/CT (p > 0.05)	Not reported
<sup>11</sup> C-choline PET/CT vs. WB-MRI <sup>118</sup>	Prospective Consecutive enrollment	1.5 T	T1/STIR/DWI	BVC Histology (n = 14)	57, BCR post-RP, 24 BCR (24LR, 27NR, 22BR)	LR: 83.3% PET/CT, 54.2% MRI, NR: 81.4% PET/CT, 77.9% MRI, BR: 92.9% PET/CT, 78.6% MRI	LR: 93.9% PET/CT, 81.8% MRI, NR: 99.7% PET/CT, 87.5% MRI, BR: 98.4% PET/CT, 87.5% MRI
<sup>68</sup> Ga-PSMA PET/CT vs. <sup>18</sup> NaF PET/CT versus WB-DWI <sup>119</sup>	Prospective Consecutive enrollment	3T	T1/T2/STIR/DWI	BVC	68, BCR post-RP (46), RP + RT (17), RT (5), BCR 10, (10 BR)	80% <sup>68</sup> Ga-PSMA PET/CT, 90% <sup>18</sup> NaF PET/CT, 25%–38% DWI	98%–100% <sup>68</sup> Ga-PSMA, 90%–98% <sup>18</sup> NaF PET/CT, 87%–92% DWI

Table 3. Continued

Imaging modality	Study design	Magnetic field strength	Sequences	Reference standard	Patients (n), status (ND, BCR), M (n)	Sensitivity (patient basis)	Specificity (patient basis)
WB-MRI vs. <sup>68</sup> Ga-PSMA PET/CT <sup>120</sup>	Prospective Consecutive enrollment	1.5T	T2FS/T2TIRM/ T1 VIBE post contrast/ ax T2TSE prostatic fossa	BVC Histology (n = 7)	28, post-RP, 20 BCR (7 LR, 5 NR, 5 BR, 2 NR + BR, 1 VR)	100% PSMA PET/CT, 55% WB-MRI, PSMA PET/CT > WB-MRI in NR	Not reported

Abbreviations: AS-MRI, axial skeleton MRI; BCa, breast cancer; BCR, biochemical relapse; BM, bone metastasis; BR, bone recurrence; BS, bone scintigraphy; BVC, best valuable comparator; DCE, dynamic contrast-enhanced imaging; DWI, diffusion-weighted imaging; FO, fat only; GRE, gradient echo pulse sequence; HASTE, half Fourier acquisition single shot turbo spin echo; LR, local recurrence; NM, not metastasis; NR, Node recurrence; PCa, prostate cancer; RP, radical prostatectomy; RT, radical radiotherapy; STIR, short tau inversion recovery; T1, T1-weighted imaging; T2, T2-weighted imaging; T1 LAVA, liver acquisition with volume acquisition; T1 VIBE, Volumetric Interpolated Breath-hold Examination; TIRM, turbo inversion recovery measurement; TXR, targeted X-rays; VM, visceral metastasis; VR, visceral recurrence (lung or liver); WB-MRI, whole-body MRI.

PET/CT compared to BS for distant metastasis were 92% versus 54% and 99% versus 93%, respectively. It should be noted that first-line PSMA detected abdominal nodal metastasis in 9% of the cohort, bone metastasis in 10%, and visceral metastasis in 1%.<sup>134</sup>

Although WB-MRI and PSMA-PET/CT appear to outperform BS for detecting bone metastases, few studies have directly compared the two methods. One study prospectively determined the diagnostic accuracy of <sup>68</sup>Ga-PSMA-PET/CT in comparison to <sup>18</sup>F-fluoride-PET/CT and WB-MRI for detecting bone metastases in patients with PCa.<sup>135</sup> More than two-thirds of the 55-patient cohort were under androgen deprivation therapy (ADT) or had castration-resistant PCa (CRPC). The patient-based diagnostic sensitivity, specificity, and overall accuracy were, respectively, 100%, 100%, and 100% for PSMA-PET/CT; 95%, 97%, and 96% for NaF-PET/CT; and 80%, 83%, and 82% for WB-MRI; the overall diagnostic accuracy of PSMA-PET/CT was significantly superior to that of WB-MRI (*p* = 0.004) but not to NaF-PET/CT (*p* = 0.48). Another study found higher sensitivity, 90%–96%, but lower specificity, 70%–90%, for <sup>18</sup>F PSMA-PET/CET compared to WB-MRI (sensitivity 43%–80%; specificity, 80%–96%).<sup>115</sup> As PSMA-PET/CT showed a relatively high number of false-positive bone lesions in this study (15%), WB-MRI may be proposed as a direct solving tool, and it may also be proposed as an alternative tool when the diagnosis of polymetastatic disease is expected on the basis of clinical and biological findings at presentation (Table 4).

Lymph node staging has always been a challenge in PCa, and despite NGI, no technique has shown an optimal performance for detecting metastatic lymph nodes. Surgical lymph node dissection (LND) is used as a gold standard and is still routinely performed and recommended during radical surgery.<sup>7,8,137</sup> However, LND has failed to improve oncologic outcomes, including survival, and lymph node invasion status only provides prognostic information.<sup>138</sup> Therefore, functional imaging, for example, DWI MRI and PET/CT, is of interest for lymph node staging. <sup>68</sup>Ga-PSMA PET/CT, because of its rapid development and promising detection rates in other stages of the disease, has been proposed for primary lymph node staging.<sup>139</sup> A recent meta-analysis found both a higher sensitivity (65% vs. 41%) and specificity (94% vs. 92%) for <sup>68</sup>Ga-PSMA PET over mpMRI in detecting pathological nodes in the pelvis,<sup>140</sup> and an analysis of 20 ND intermediate- and high-risk patients with PCa who underwent <sup>68</sup>Ga-PSMA-11 PET/CT, anatomical MRI or contrast-enhanced CT, and DWI-MRI prior to laparoscopic, template-based, extended LND showed that the sensitivity and specificity for detecting lymph node metastases were, respectively, 39% and 100% with <sup>68</sup>Ga-PSMA PET/CT, 8% and 100% with MRI/CT, and 36% and 83% with DWI-MRI.<sup>139</sup>

**Table 4. Current clinical positioning of whole-body magnetic resonance imaging (WB-MRI) in prostate cancer (PCa)**

Newly diagnosed PCa
Consider WB-MRI:
After equivocal conventional imaging (unconfirmed BS findings, CT, or MRI)
After negative conventional imaging (BS, CT, or MRI) in unfavorable intermediate or high/very high risk PCa
As a problem-solving tool in patients with ambiguous findings at PET/CT screening (numerous false positives of PSMA-PET/CT <sup>115</sup> )
As a first line “all in one” screening approach (local, regional, global) for locally advanced or high-risk disease
In de novo OMD by conventional imaging being considered for ablative therapy: validation–invalidation tool = accurate diagnosis > > > role for metastasis directed therapy
Along with PET/CT for confident and comprehensive diagnosis of OMD: combinatorial approach <sup>136</sup>
Alternative to conventional imaging if PMD is expected, as baseline before the start of systemic treatment, for future therapy response assessments
Biochemical recurrence
Consider WB-MRI:
After conventional imaging (BS, CT, or MRI) or PSMA-PET/CT if they are negative or equivocal in high-risk patients suitable for salvage pelvic or distant therapy
If no access to PSMA-PET/CT <sup>126</sup>
Castration-resistant prostate cancer
Consider WB-MRI:
Before initiating a new treatment: evaluate disease presence, extent, distribution, and as baseline for future response assessments
At follow-up: therapy response assessment using MET-RADS-P criteria
To select bone and soft-tissue biopsy sites for approved genomic directed therapies
Abbreviations: OMD, oligometastatic disease; PMD, polymetastatic disease.

### Biochemical Recurrence (Table 5)

The American Urological Association (AUA) defines BCR after radical prostatectomy (RP) as a detection of increasing PSA > 0.2 ng/mL on two consecutive tests and defines BCR after radiotherapy as an increase in PSA level 2 ng/mL above PSA nadir.<sup>141</sup>

Salvage local treatment is often applied in selected patients. Because most patients do not show metastases on standard imaging assessment, the decision to start systemic treatment was mostly based on PSA kinetics. Recent developments in NGI revealed that a fair proportion of these patients was actually harboring limited metastatic spread using WB-MRI, often occurring outside the pelvic region, and this result challenged the concept of salvage pelvic treatment. For example, an assessment of metastatic spread showed that more than two-thirds of 96 patients with metastatic disease had lesions located outside the usually recommended targets of extended pelvic LND (eLND) and external beam radiation therapy (EBRT).<sup>142</sup>

NGI has profoundly modified the approach to BCR. An earlier and more precise assessment of metastatic deposit allows a better selection of patients for salvage local treatment or further surveillance. As for those with limited metastatic deposit, intervention with MDT, mostly by stereotaxic ablative radiation (SABR), delays progression.<sup>128</sup> In the ORIOLE Phase 2 Randomized Clinical Trial, 54 men with recurrent hormone-sensitive PCa and one to three metastases detectable by conventional imaging were randomized to receive systemic treatment alone or in combination with SABR. Treatment with SABR improved median progression-free survival (not reached vs. 5.8 months; hazard ratio, 0.30; 95% confidence interval, 0.11–0.81;  $p = 0.002$ ).<sup>143</sup> The most interesting observation was that total consolidation of PSMA radiotracer decreased the risk of new lesions at 6 months (16% vs. 63%;  $p = 0.006$ ), thus confirming the importance of accurate imaging staging by PSMA PET/CT.

At BCR, PSMA PET/CT has become the technique of choice. European Association of Urology (EAU) guidelines

**Table 5. Indications for imaging workup at biochemical recurrence (BCR)**

Post-RP (two consecutives rising prostate-specific antigen [PSA] >0.2 ng/mL)
EAU
If PSA level >0.2 ng/mL and results influence treatment decisions: PSMA PET/CT
If PSA level >1 ng/mL, PSMA PET/CT is not available, and results influence treatment decisions case: <sup>18</sup> F-Fluciclovine or <sup>11</sup> C-choline PET/CT.
NCCN
Bone imaging, chest CT, abdominopelvic CT or MRI.
<sup>18</sup> F-NaF or <sup>11</sup> C-choline or <sup>18</sup> F-Fluciclovine PET/CT or PET/MRI can be considered after BS if high clinical suspicion of metastasis.
Post-RT (any PSA increase ≥2 ng/mL higher than PSA nadir value)
EAU
In patients who are candidates for local salvage therapy: prostate mpMRI
In patients who are candidates for curative salvage treatment: PSMA PET/CT (if available) or <sup>18</sup> F-Fluciclovine PET/CT or <sup>11</sup> C-choline PET/CT.
NCCN
In patients who are candidates for local therapy: prostate mpMRI, BS, chest CT, abdominopelvic CT/MRI.
<sup>18</sup> F-NaF or <sup>11</sup> C-choline or <sup>18</sup> F-fluciclovine PET/CT or PET/MRI can be considered after BS when clinical suspicion of metastasis is high.
In patients who are not candidates for local therapy: BS.
<sup>18</sup> F-NaF or <sup>11</sup> C-choline or <sup>18</sup> F-fluciclovine PET/CT or PET/MRI can be considered after bone scan when clinical suspicion of metastasis is high.
<i>Note:</i> Recommendations are based on European Association of Urology, European Society for Radiotherapy and Oncology, and International Society of Geriatric Oncology (EAU-ESTRO-SIOG) guidelines 2019, and National Comprehensive Cancer Network (NCCN) guidelines, version 2.2020. Abbreviations: <sup>11</sup> C-choline, carbon-11-choline; <sup>18</sup> F-Fluciclovine, <sup>18</sup> F-FACBC; <sup>18</sup> F-NaF, fluorine 18–sodium fluoride; mpMRI, multi-parametric MRI; RP, radical prostatectomy; RT, radical radiotherapy.

recommend performing PSMA PET/CT in patients with relapse PSA >0.2 ng/mL after RP or, in case of unavailability of PSMA PET/CT and a PSA level ≥ 1 ng/mL, fluciclovine choline PET-CT is used. After radiotherapy, guidelines recommend performing prostate gland mpMRI to localize abnormal areas and guide further biopsies (Table 5) (Figure 5). WB-MRI has not been widely evaluated in BCR because of its limited value for the detection of early metastatic involvement in normal-sized lymph nodes. The vast majority of experts at the St. Gallen Advanced Prostate Cancer Consensus Conference (APCCC) 2019 recommended performing <sup>68</sup>Ga PSMA PET-CT +/- mpMRI rather than WB-MRI in patients with BCR after RP or RT.

One retrospective report described the potential use of WB-MRI combined with mpMRI in BCR after RP in 76 patients with low PSA level (median, 0.36 ng/mL).<sup>144</sup> WB-MRI with mpMRI identified recurrence in 21% and

local recurrence in 9% of the patients. MRI was found to be a feasible modality for clinical practice and provided incremental information compared to conventional imaging (Figure 5). Due to the high lesion to background contrast of DWI, compared to anatomical sequences, the detection of distant metastasis, except sclerotic bone metastasis, should be facilitated by DWI.<sup>145</sup> The LOCATE trial is comparing WB-MRI to conventional imaging (BS and CT) in a cohort of 213 patients for detecting nodes and bone metastasis in BCR after radiotherapy.<sup>146</sup>

The diagnostic accuracies of <sup>68</sup>Ga-PSMA PET/CT, <sup>18</sup>F-NaF PET/CT, and DWI-MRI for the detection of BM were prospectively compared in 68 patients with BCR.<sup>119</sup> On a patient level, sensitivity and specificity were, respectively, 0.80 and 0.98–1.00 for <sup>68</sup>Ga-PSMA PET/CT, 0.90 and 0.90–0.98 for <sup>18</sup>F-NaF PET/CT, and 0.25–0.38 and 0.87–0.92 for DW<sub>600</sub>-MRI. The diagnostic performance of

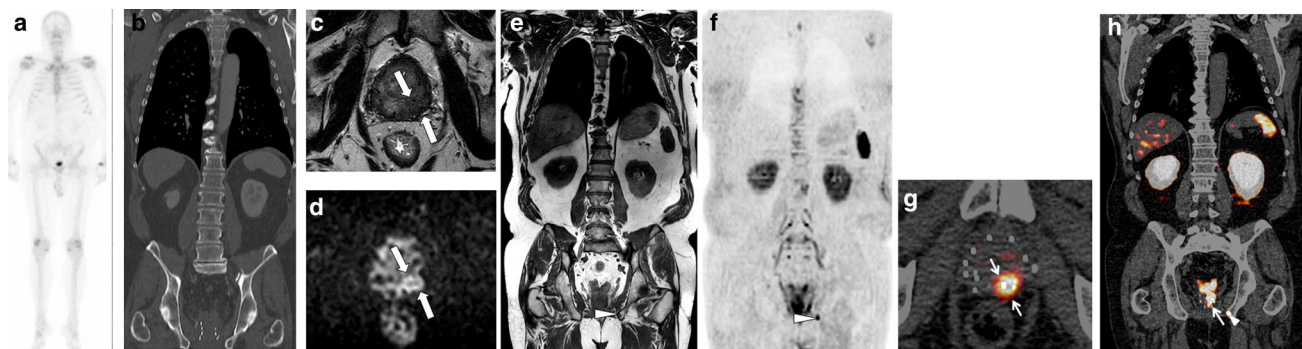


**Figure 5:** “All in one” whole-body magnetic resonance imaging (WB-MRI) and  $^{68}\text{Ga}$  PSMA PET/CT workup at BCR in a 65-year-old man with rapid rising prostate-specific antigen (PSA) 2 years after brachytherapy (5.84 ng/mL) shows intraprostatic and oligometastatic bone recurrence. (a, b) Normal AP bone scintigraphy (a) and coronal MPR thoracoabdominal CT image (b) show no abnormality. (c–f) All-in-one WB-MRI at 3T: (c, d) mpMRI, transverse T2 TSE (c) and DWI (b 1500 s/mm<sup>2</sup>) (d) images show intraprostatic recurrence (arrows) with low SI on T2 and restricted diffusion on DWI; coronal 3D T1 FSE (e) and DWI (b 1000 s/mm<sup>2</sup>, inverted grayscale) (f) images show a single bone metastasis in the left ischiatic bone (arrowhead) of low SI on T1 (e) and high signal on DWI (f). (g, h) Fused  $^{68}\text{Ga}$  PSMA PET/CT images: transverse section at the level of the prostate (g) and coronal MPR image (h) show intraprostatic recurrence (arrows in g and h) with focal high uptake (SUV max 6.92) and focal left ischiatic bone metastasis (arrowhead in H) (SUV max 13.88). Patient was treated with stereotactic radiotherapy on both bone and prostate lesions and 6 months of ADT with subsequent drop in PSA level at <0.2 ng/mL.

DWI-MRI was significantly lower than that of  $^{68}\text{Ga}$ -PSMA PET/CT and  $^{18}\text{NaF}$  PET/CT for diagnosing bone metastases.  $^{68}\text{Ga}$ -PSMA PET/CT showed a higher detection rate (100%) than WB-MRI (23%) for lesions in 28 patients with BCR following RP.<sup>120</sup>

### Advanced Disease and Response Assessment

Imaging plays an intrinsic role in defining the metastatic state (M1) when PSA increases in patients with normal testosterone levels (hormone sensitive state) or when a patient has suppressed testosterone levels (castration-resistant state). Imaging also has important roles to play when men with metastatic disease undergo treatment to assess response to therapy and also to detect the emergence of primary or secondary therapy resistance. In both hormonal states, the volume and distribution of metastases are highly prognostic and can affect therapy options.

Therapy options for the treatment of advanced metastatic disease continue to evolve, and a layered approach is often employed (Figure 6). Treatments include drugs targeting the androgen axis (enzalutamide, abiraterone, darolutamide, apalutamide), chemotherapy (docetaxel, cabazitaxel), and bone-seeking agents including bisphosphonates and <sup>223</sup>radium. More recently, drugs targeting poly(ADP)-ribose polymerase (PARP) and immunotherapy have been introduced. In the short term, we can expect to see the successful deployment of anti-PSMA directed therapies. When faced with these different therapeutic options, the evaluation of therapy response in metastatic patients is crucial for deciding whether to continue, adapt, or change treatment strategies.<sup>147</sup>

Quantitative measurements tools have been validated for assessing the effectiveness of cancer therapy in soft-tissue lesions using CT<sup>148</sup>; however, CT is ineffective for assessing

response to therapy in bones because it relies on bone reaction rather than assessing the tumor itself.<sup>6</sup>

BS is still recommended to assess bone disease response in patients with metastatic CRPC (mCRPC),<sup>7</sup> but it suffers from major limitations. The “flare phenomenon” (pseudoprogession), defined by the development of new uptake foci on an early follow-up BS and due to osteoblastic reaction, can occur within 8–12 weeks of treatment initiation.<sup>149</sup> Hence, Prostate Cancer Working Group 3 defines imaging progression in mCRPC based on BS as the appearance of  $\geq 2$  lesions during treatment continuation and confirmed 6 weeks later by a second BS. This considerably lengthens decision times and can cause the continuation of ineffective and potentially toxic treatment.<sup>150</sup> Furthermore, BS progression only relies on the emergence of new lesions and does not account for an increase in the size of preexisting lesions.<sup>151</sup> Finally, patients with diffuse metastatic bone disease on BS (so-called superscans) cannot be monitored because new lesions cannot be identified in the background of diffusely elevated tracer uptake.<sup>6</sup>

Nodes and visceral metastasis detected by abdominopelvic CT or MRI must be recorded and quantified and followed per RECIST.<sup>152</sup> For PCWG3, nodes are considered pathological when they are between 10 mm and 15 mm on the short axis and are subject to clinical discretion, but they are only considered measurable when they are over 15 mm in size.<sup>150</sup>

MRI provides the opportunity to assess the response to therapy in bone lesions, the most frequent metastatic site in mCRPC and one that cannot be correctly evaluated with standard imaging tests.<sup>153</sup> The feasibility and the value of size criteria determined using axial skeleton MRI to quantify bone metastasis and measure tumor response have been demonstrated.<sup>154</sup>

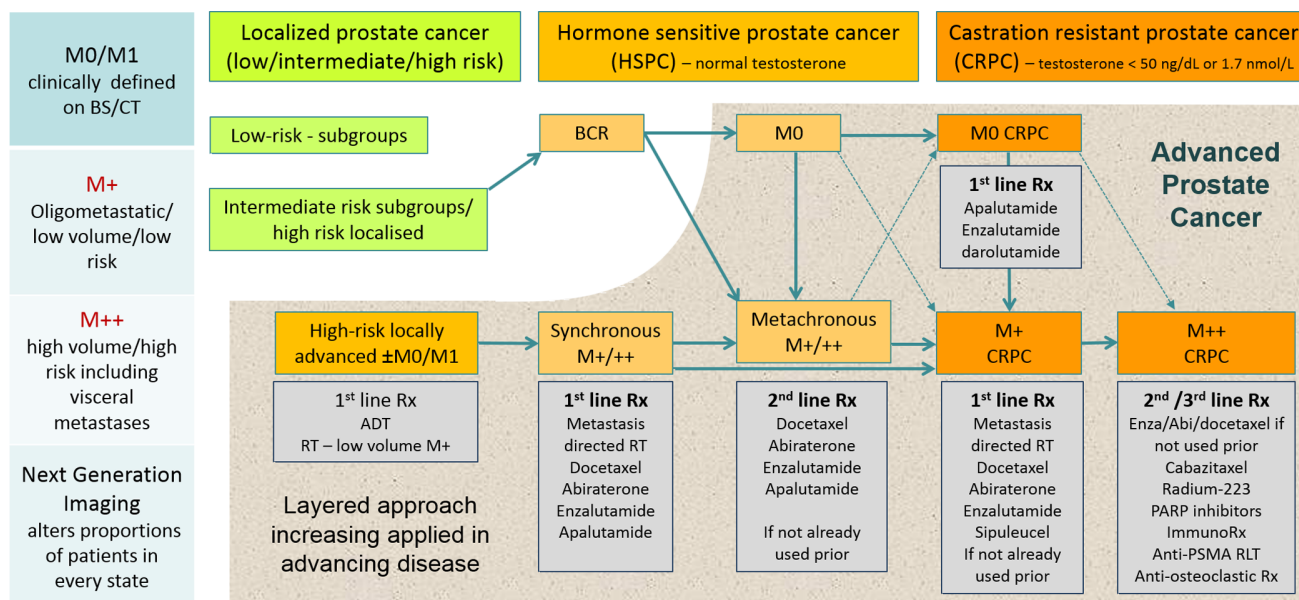


**Figure 6: Substantial progress is being made in the management of bone metastatic disease in prostate cancers. Optimal management of metastatic bone disease utilizes a layered approach as more potential treatments are added to the armamentarium. Choosing the right treatment, for the right patient, for the right duration and the correct sequence and combination remain challenges that next-generation imaging (NGI) may help to inform**

Response assessment with WB-MRI relies on an mp approach combining anatomical and functional sequences (Table 6). Response to therapy can be characterized quantitatively by a decrease in the number and size of detectable lesions and can be characterized qualitatively by a replacement of the peripheral zone of lesion by fat cells, creating a “fatty halo sign,” followed by a return of normal-appearing bone marrow.<sup>38</sup> Potential limitations of anatomical sequences in the evaluation of treatment response are the difficult interpretation of residual low-signal tissue on T1-weighted images, which may represent inactive lesions due to fibrosis or necrosis, and also a rare “flare phenomenon” corresponding to an increase in diameter of the lesion on T1 images due to edema posttherapy.<sup>160</sup> Another potential limitation is the reconversion of yellow bone marrow to red bone marrow during the treatment, leading to diffuse “pseudoprogression.”<sup>160</sup>

Thus, bone lesions must also be assessed qualitatively or quantitatively using functional DWI-MRI sequences or total DWI (tDV) measurements.<sup>73</sup> A decrease in the SI of lesions on high b-value images and an increase in ADC measured on ADC maps may be indicative of response (Figure 7). Lesions responding to systemic or radiation therapy may, however, present an increased SI on high b-value DWI with a corresponding increase in ADC values, known as the “T2 shine-through effect,” resulting from increase in water content due to necrosis or edema.<sup>161</sup> Quantitative assessment relies on ADC measurement (ADC<sub>mean</sub>, ADC<sub>slow</sub> without the perfusion effect of lower b-values) and global ADC (gADC) in case of total DWI.

MET-RADS-P defines criteria for the assessment of response in metastatic PCa, using mpMRI to reliably evaluate

the likelihood of the effectiveness of a treatment using a Likert-like category scale from 1 to 5, where category 1 indicates very high likelihood of response and 5 indicates high likelihood of progression. Category 3 indicates stable disease. Bone disease response is divided into progression, stable disease, response, and discordant categories. Soft-tissue disease is recorded using RECIST 1.1 criteria. MET-RADS-P is still being evaluated in clinical practice, as well as clinical trials, to assess its impact on the care pathway for advanced PCa.<sup>162</sup> One study assessed the value of MET-RADS-P criteria in 72 patients with mCRPC when disease progression was suspected at the start of a new line of treatment and found that a high number of bone (≥10) and visceral metastases, as determined by MET-RADS-P, was significantly associated with shorter cancer-specific survival.<sup>163</sup> This suggests the potential value of MET-RADS-P volume score as a prognostic biomarker.

A retrospective study found that some lesions in responder (13%) and nonresponder patients (13%) presented a decrease in ADC values, while other lesions had increased ADC.<sup>156</sup> MET-RADS-P offers the possibility to record these heterogeneous observations in their response evaluation and categorizes the response as discordant if some soft-tissue or bone lesions are progressing without meeting the criteria of progression of disease, while others are stable or are responding<sup>162</sup> (Figure 7).

WB-MRI does not rely on the affinity of tumor cells for a tracer or on the presence of receptors, and this makes it a consistent and universal tool for response assessment. PSMA PET/CT, which has been shown to be very efficient at BCR and in newly diagnosed disease for detection, should be

**Table 6. Value of whole-body magnetic resonance imaging (WB-MRI) for response assessment in metastatic prostate cancer (PCa) at 1.5T**

Sequences	Study design	Coverage	Approach	Reference standard	Patient characteristics	Results
T1/T2W FSE <sup>154</sup>	Prospective consecutive enrollment	Axial skeleton	RECIST-like	BVC	20 eligible mCRPC patients, 13 NM, 22BM, 1 VM, imaging before and after therapy (6 m)	Number of measurable lesions compared to CT (30%–66%), CR = 2, PR = 2, SD = 5, PD = 11
DWI SPIR/T2 FSE <sup>155</sup>	Prospective consecutive enrollment	Axial skeleton	Quantitative mean ADC correlated with PSA levels, DM/ADC voxel	NR	9 patients, 20 BM, imaging before and after therapy (1, 2, 3 m)	Response of BM to ADT: ↑ mean ADC (15%–27%) correlated with ↓ PSA level (r = -0.439). Spatial heterogeneity within lesion, DM analysis: 47.3% voxels ↑ ADC
DWI T1/T2 FSE <sup>156</sup>	Prospective consecutive enrollment	Axial skeleton	Quantitative ADC-ADC <sub>slow</sub>	PSA RECIST	26 patients, 6 BM + ST, 20 BM, imaging before and after therapy (12 weeks)	Responders: ↑ mean ADC (52.5%), ADC <sub>slow</sub> (35.8%); Nonresponders: ↑ mean ADC (19%) and ADC <sub>slow</sub> (16.7%), mean ADC = not appropriate measurement tool of bone response
DWI T1 GRE <sup>157</sup>	Prospective consecutive enrollment	WB-MRI	Quantitative tDV/gADC	BVC	4 BCa- 7 PCa, 7 BM, imaging before and after therapy (12–38 weeks)	Responders: ↓ tDV (-85% to +27%), ↑ gADC (-0.07 to +0.78); Nonresponders: ↑ tDV (3%–284%), stable gADC (-0.10 to +0.05)
DWI T1 GRE <sup>158</sup>	Retrospective	WB-MRI	Correlation tDV with OS and PF (Hb, PSA, LD, ALP level)	OS	43 eligible mCRPC patients, 20 BM, 17 BM + NM, 6 BM + VM, imaging before and after therapy (1 y)	↑ TDV = poor OS (HR: 1.74). Correlation between tDV and PF; Hb level: r = -0.521, PSA level: r = 0.556, LD level: r = 0.534, ALP: r = 0.572
DWI T1 GRE <sup>159</sup>	Prospective consecutive enrollment	WB-MRI	RECIST 1.1, Quantitative tDV, mean ADC	RECIST 1.1	21 mCRPC patients, 21BM, 12BM + NM, 11 BM + VM, Imaging	Responders: ↓ tDV (5.6%–58.8%) ↓ Nonresponders: ↑ tDV (0%–76.9%), volume of 5 target lesions associated with

Table 6. Continued

Sequences	Study design	Coverage	Approach	Reference standard	Patient characteristics	Results
					before and after therapy (12 weeks)	response (OR = 0.89; 95% CI: 0.80, 0.99)

Abbreviations: ADC<sub>slow</sub>, ADC without the effect of perfusion; ADT, androgen deprivation therapy; ALP, alkaline phosphatase; BCa, breast cancer; BM, bone metastasis; CR, complete response; CT, computed tomography; DM, functional diffusion map; gADC, global ADC; Hb, hemoglobin; HR, hazard ratio; LD, lactate dehydrogenase; mCRPC, metastatic castration-resistant prostate cancer; NM, node metastasis; NR, not reported; OR, odds ratio; OS, overall survival; PD, progressive disease; PF, prognosis factors; PR, partial response; r, Pearson correlation coefficient; SD, stable disease; ST, soft tissue metastasis; T, Tesla; tDV, total diffusion volume; VM, visceral metastasis.

considered with caution for response evaluation at the CRPC stage not only because it shows variable affinity but because this affinity may vary with the line and type of treatment. The interaction between androgen signaling and PSMA expression is quite complex and still under evaluation. Prolonged androgen blockade (AB) leads to the downregulation of PSMA expression, reducing the visibility and the possibility of following metastatic PCa lesions on PSMA-PET/CT.<sup>164</sup> Conversely, short-term AB rapidly upregulates PSMA expression in CRPC, leading to a flare effect. This flare phenomenon does not seem to be as transient compared to BS, and it could plateau and lead to the misinterpretation of false progressive lesions.<sup>165,166</sup> Experts recommend performing PSMA-PET/CT before the start of treatment and not earlier than 3 months after initiating systemic therapy and, most importantly, agree to not routinely follow PCa patients with PSMA PET/CT.<sup>10</sup> Precise and reproducible criteria (akin to MET-RADS-P) for evaluating therapy response with PSMA PET/CT are needed to standardize interpretations, and reporting of PET/CT is required to decrease inter- and intraobserver variability.<sup>167</sup>

### Current Developments and Future Perspectives

#### “All in One” PCa Staging: Combining mpMRI and WB-MRI

An “all in one” MRI approach of PCa consists of a single MRI examination combining diagnostic mpMRI of the prostate for locoregional staging with WB-MRI for node and general metastatic staging. Both mpMRI and WB-MRI acquisitions have been accelerated to make such an “all in one” imaging approach possible. PI-RADS v.2 guidelines have reduced the importance of the DCE sequence for the characterization of PCa, with others showing low value of the full mpMRI approach for men with clinically obvious locally advanced disease at presentation.<sup>168</sup> This has led to the development of a biparametric approach relying on T2 and DWI sequences for local disease detection, biopsy planning, and staging.<sup>169</sup> A recent meta-analysis of 31 studies for the detection of PCa in naïve patients demonstrated no statistical differences between biparametric MRI and mpMRI in terms of sensitivity and specificity.<sup>170</sup>

We have already noted that the use of 3D or Dixon imaging decreases the number of necessary anatomical sequences for WB-MRI examinations. This reduces the acquisition time of the “all in one” protocol combining bpMRI of the prostate and WB-MRI (WB 3D T1GREMDixon and DWI sequence) to less than 40 min. This protocol enables a one-step tumor node metastasis (TNM) staging and is mostly relevant in men with newly diagnosed, high-risk locally advanced and high-risk BCR

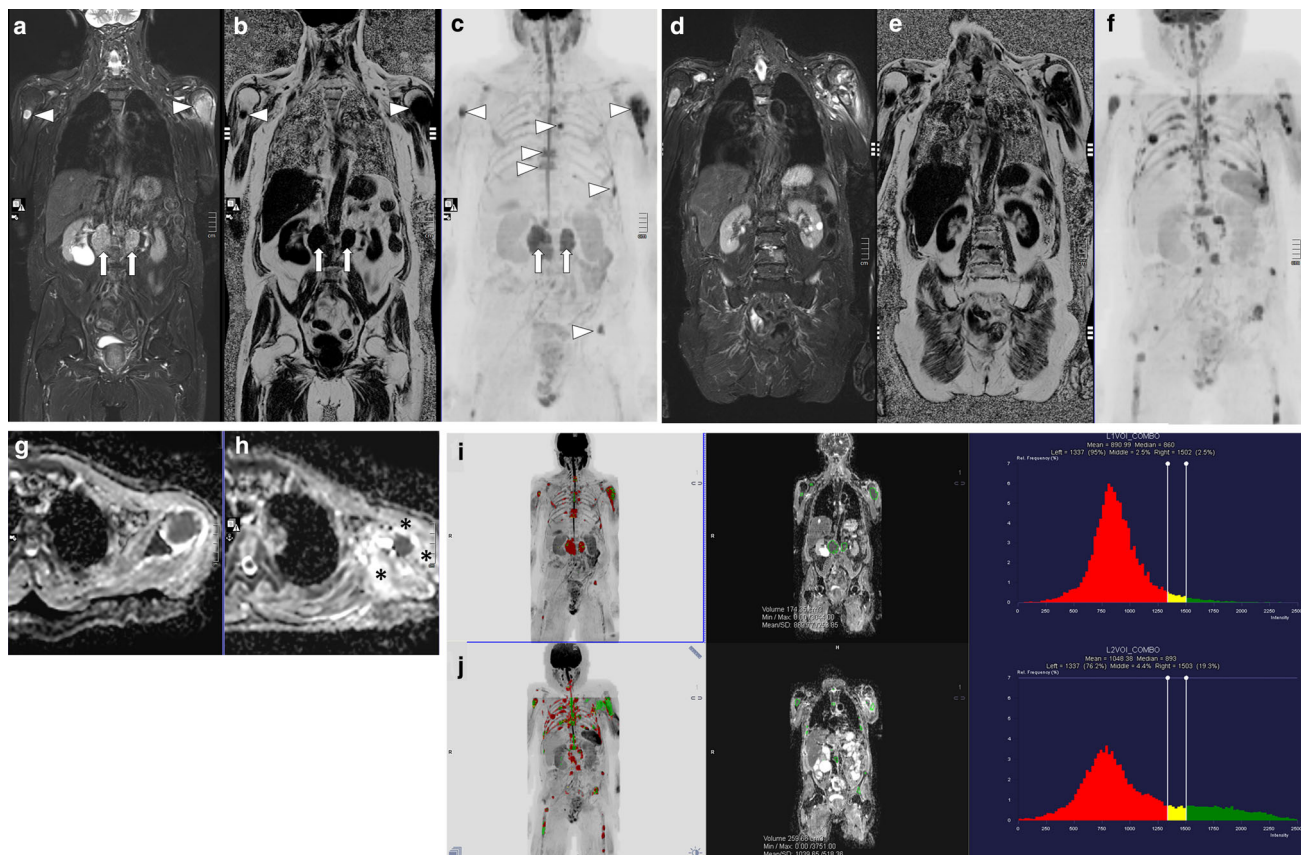


**Figure 7:** A 74-year-old man with metastatic castration-resistant prostate cancer (PCa). Prior androgen deprivation therapy (ADT) and pelvic radiotherapy for node-positive Gleason 3 + 3 prostate cancer. Previous docetaxel chemotherapy for metastatic castration-resistant PCa (mCRPC). Baseline whole-body magnetic resonance imaging (WB-MRI) and 3-m follow up on androgen receptor directed therapy (enzalutamide). (a–c) Baseline (BL) WB-MRI. Coronal water-only T2 Dixon (a), F% (b), and b 900 s/mm<sup>2</sup> diffusion-weighted imaging (DWI) (c) (maximal intensity projection [MIP]; inverted grayscale) images show retroperitoneal nodal enlargement (vertical up arrows) and multiple bone deposits (horizontal arrowheads). A left humeral expansive metastasis with extraosseous soft tissue disease is seen, suggesting significant fracture risk. (d–f) Follow-up (FU) WB-MRI shows corresponding images after enzalutamide therapy. A “mixed” response is observed with significant reduction in the size of the retroperitoneal lymphadenopathy but marked skeletal progression with increase in number and size of bone lesions. Fracture of the left humerus is seen with edema of the surrounding soft tissues. Note that there was no intervening shoulder radiotherapy. (g, h) Comparison of BL (g) and FU (h) axial ADC maps shows preserved malignant signal within the fractured humerus but marked edema of the surrounding soft-tissue following the fracture (\*). (i, j) Comparison of BL (i) and FU on therapy (j) examinations by quantitative MRI. WB tumor load segmentation undertaken on syngo via onco-trend software (Siemens Healthineers, Erlangen, Germany). The MIP images on the high b-value (900 s/mm<sup>2</sup>) are overlaid with ADC value color classes using the thresholds indicated on the histograms. The green voxels are values  $\geq 1500 \mu\text{m}^2/\text{s}$  (voxels that are “highly likely” to be responding). The yellow voxels are set to lie between the 95th centile ADC value of the pretreatment histogram ( $1337 \mu\text{m}^2/\text{s}$ ) and  $1500 \mu\text{m}^2/\text{s}$  (voxels “likely” to be responding). Red voxels represent mostly untreated and still active disease. An increase in the volume of the active (red voxels) disease is measured (166 mL [95% of 174 mL before therapy] and 198 mL [76.2% of 259.7 mL after therapy]). The increase in mean ADC due to increasing numbers of green voxels located mostly in the left shoulder region is due to the fracture-related edema, but there is also some response of the bone disease in the right femur and left iliac bone. Mixed responses between tissues (in this case, between nodes versus bone) and within tissues (bones) strongly indicates that secondary resistance is due to Darwinian selection pressures. This phenomenon is commonly seen in men with castration-resistant prostate cancer being treated with targeted therapies. WB-MRI can enable the identification of skeletal sites at high risk of developing adverse events such as fractures even if they are asymptomatic

PCa to guide the choice between local or systemic treatment (Figure 6, Table 7).

**Oligometastatic Disease**

NGI allow the recognition of some patients with a low volume of metastases to be defined as patients with oligometastatic disease (OMD) either at diagnosis, BCR, or

after treatment. First described using BS,<sup>171</sup> the current definition of oligometastases consists of three to five lesions (usually node or bone) detected with NGI, including PET/CT and WB-MRI.<sup>172</sup> In patients with ND PCa or BCR, the role of imaging is to truly discriminate patients with OMD who can potentially benefit from extended radical treatment or salvage with MDT from polymetastatic patients who require

**Table 7. Research indications for whole-body magnetic resonance imaging (WB-MRI) in prostate cancer (PCa)**

Newly diagnosed PCa
De Novo OMD detected by conventional imaging: use WB-MRI as a validation–invalidation tool, adjunct to PSMA-PET/CT, to validate the use of local treatment with MDT + ADT.
In case of de novo polymetastatic PCa detected by conventional imaging: use DWI WB-MRI to optimize therapy response assessment in the follow-up.
Fast “all in one” screening approach: first line, quick, effective, nonirradiating “triage tool” for unfavorable intermediate/high to very high risk PCa.
Integrate hybrid PET/MRI modalities in primary staging.
Biochemical recurrence
Integrate hybrid PET/MRI modalities in BCR restaging.
As a prognostic marker to distinguish candidate lower-risk patients for PSA-directed surveillance versus high risk for ADT + MDT.
Castrate-Resistant Prostate Cancer: use WB-MRI
As a prognostic marker to distinguish candidate patients for surveillance or ARPI + MDT after negative conventional imaging (nmCRPC).
To confirm OMD CRPC to validate the use of MDT in addition of ARPI.
To evaluate homogeneity or heterogeneity of disease response/progression before initiating any subsequent treatment.
As a biomarker to assess therapy response regarding concordance or discordance with biology or clinical features.
To assess total tumor load when selecting patients for anti-PSMA directed therapies (theragnostic role)
Abbreviations: ADT, androgen deprivation therapy; ARPI, androgen receptor pathway inhibitor; BCR, biochemical recurrence; MDT, metastasis-directed therapy; MET-RADS-P, metastasis reporting and data system for prostate cancer; nmCRPC, nonmetastatic castration resistant prostate cancer; OMD, oligometastatic disease; PMD, polymetastatic disease.

systemic therapy. In a cohort of 96 patients with metastatic ND PCa, WB-MRI identified patients with OMD in 28% of the metastatic hormone-naïve PCa and in 52% of the mCRPC.<sup>142</sup>

The scientific community has recently used PET/CT (<sup>18</sup>F-Na or PSMA) or WB-MRI to stage ND disease in case of negative or equivocal results with conventional imaging tests and in BCR in case of salvage local therapy to ensure that there is no distant metastasis.<sup>126</sup> The potential impact of NGI in the selection of these patients and in long-term outcomes is not yet clearly understood and deserves further study, although patients benefiting from MDT have better ADT-free survival rates.<sup>142,173–177</sup> There is no evidence that the primary treatment influences the metachronous metastatic status (oligo vs. polymetastatic).<sup>178</sup>

As previously mentioned, functional PET imaging and high-contrast MRI are complementary, and hybrid PET/MRI outperforms PET/CT or MRI alone in staging and in BCR patients.<sup>179–183</sup> A combination of both techniques may allow better identification of patients with OMD at the ND or BCR, which is fundamental for the effective treatment of men with OMD.

## HYBRID PET/MRI: THE BEST OF BOTH WORLDS

PSMA PET/CT and WB-MRI appear to be the techniques of choice for staging and evaluating recurrence in PCa. Therefore, PSMA PET/MRI could be of clinical interest as it combines the best abilities of both techniques, provided that PET/MRI scanners can perform the most effective MRI sequences with quality similar to that of standalone MRI systems.

Hybrid PET/MRI combines functional assessment with the sensitivity of DWI and specificity of PET tracers and with the high-contrast resolution and anatomical detail of MRI (Figure 8). It is performed at 3T and obtains T2- (T2SSFE/HASTE) and T1 Dixon images and DWI sequences.<sup>184,185</sup> After intravenous injection of the PET tracer, emitted 511-keV photons from the radiotracers undergo attenuation through the body before being detected. A key step in obtaining high-quality images and the accurate calculation of standardized uptake values (SUV) is to correct the attenuation effect of the photons via attenuation correction maps. In PET/CT, this correction is done with CT attenuation values. In PET/MRI, MR-based attenuation correction (MRAC)

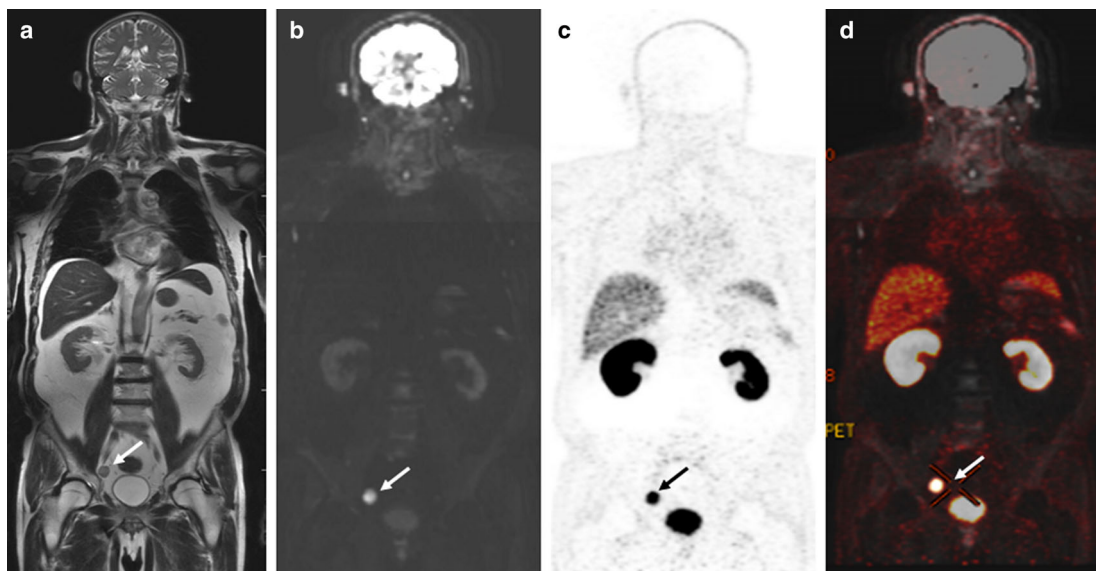


**Figure 8:** Prostate-specific membrane antigen (PSMA)-positron emission tomography (PET)/magnetic resonance imaging (MRI) at biochemical recurrence in a 56-year-old man with rising prostate-specific antigen (PSA) (2,2 ng/mL) after prostatectomy. (a) Coronal T2W image shows enlarged right iliac lymphadenopathy (arrow). (b) Coronal diffusion-weighted imaging (DWI) (b 1000) confirms nodal recurrence. (c) Simultaneous PET image shows increased PSMA uptake. (d) Image fusion of DWI and PSMA-PET shows the coherence of both techniques

maps are based on a breath-hold two-point Dixon Volumetric Interpolated Breath-hold Examination (VIBE) sequence that generates water and FF signal with different frequencies.<sup>186</sup>

Recent works demonstrated better results using PET/MRI compared to mpMRI of the prostate for local staging.<sup>179–181</sup> In studies comparing PET/MRI to PET/CT, either using Ga-PSMA-11 (81% of studies) or 11C-choline (19% of studies), PET/MRI appeared more accurate for detecting local recurrences and slightly better for detecting nodal metastases.<sup>187</sup> MRI was crucial for the better detection of local recurrences, and the longer tracer accumulation at PET/MRI was likely responsible for the better lymph node staging. As for detecting bone metastases, there is no advantage to either imaging technique.

A current important limitation is the duration of PET/MRI examinations compared to PET/CT (60 min vs. 20 min). This depends on the inclusion of dedicated pelvic and mp sequences and can make its integration in clinical practice difficult. Going forward, it will be important to determine the specific indications where PET/MRI would deliver information critical for treatment selections or prognostication in order to justify the higher costs for PET/MRI. Nevertheless, hybrid PET/MRI provides a unique research opportunity to compare differences and complementary values of PSMA PET and WB-MRI techniques at different stages of PCa and for the development of new tracers such as <sup>18</sup>F-labeled PSMA radiopharmaceuticals with longer half-lives, which enable higher spatial resolution images with different biodistributions; <sup>18</sup>F 16-βfluoro-5-α-dihydrotestosterone (FDHT), which binds to the intracellular androgen receptor; and <sup>18</sup>F fluciclovine, which takes advantage of upregulated glutamate transporters in PCa.<sup>3</sup>

The use of PET/MRI appears promising at BCR, and the superiority of <sup>68</sup>Ga PET-CT/mpMRI compared to <sup>68</sup>Ga PSMA-PET/CT alone for local recurrence assessment was demonstrated in two studies.<sup>183,188</sup>

## CONCLUSION

Accurate staging and assessment of disease response to therapies are the two main expectations for imaging in the era of high-precision oncology. NGI modalities now stand beside conventional imaging techniques in guidelines recommending imaging use at the various stages of PCa. Currently, NGI modalities mostly include WB-MRI and PSMA PET/CT. In the future, we can expect the increasing use of NGI methods in clinical practice because of improved disease detection sensitivity and more accurate response assessments compared to BS and CT. The impacts on patients' outcomes resulting from the reclassification of patients using NGI methods, combined with improved therapeutics, are yet to be determined.

## ACKNOWLEDGMENTS

The authors acknowledge John William Bean, PhD (Bean Medical Writing, Halle, Belgium) for providing medical writing services. Funded by Grant Support: Personalized Medicine and Integrated Care: the MOC-UP Project (CONVENTION INNOVIRIS 2017-PFS-15)

## References

1. Burdett S, Boeve LM, Ingleby FC, Fisher DJ, Rydzewska LH, Vale CL, et al. Prostate radiotherapy for metastatic hormone-sensitive prostate

- cancer: a STOPCAP systematic review and meta-analysis. *Eur Urol*. 2019;76(1):115–24.
2. Bray F, Ferlay J, Soerjomataram I, Siegel RL, Torre LA, Jemal A. Global cancer statistics 2018: GLOBOCAN estimates of incidence and mortality worldwide for 36 cancers in 185 countries. *CA Cancer J Clin*. 2018;68(6):394–424.
  3. Perez-Lopez R, Tunariu N, Padhani AR, Oyen WJG, Fanti S, Vargas HA, et al. Imaging diagnosis and follow-up of advanced prostate cancer: clinical perspectives and state of the art. *Radiology*. 2019;292(2):273–86.
  4. Blackledge MD, Tunariu N, Zungi F, Holbrey R, Orton MR, Ribeiro A, et al. Noise-corrected, exponentially weighted, diffusion-weighted MRI (niceDWI) improves image signal uniformity in whole-body imaging of metastatic prostate cancer. *Front Oncol*. 2020;10:704.
  5. Ghafoor S, Burger IA, Vargas AH. Multimodality imaging of prostate cancer. *J Nucl Med*. 2019;60(10):1350–8.
  6. Padhani AR, Lecouvet FE, Tunariu N, Koh DM, de Keyzer F, Collins DJ, et al. Rationale for modernising imaging in advanced prostate cancer. *Eur Urol Focus*. 2017;3(2–3):223–39.
  7. Mohler JL, Antonarakis ES, Armstrong AJ, D’Amico AV, Davis BJ, Dorff T, et al. Prostate cancer, version 2.2019, NCCN clinical practice guidelines in oncology. *J Natl Compr Canc Netw*. 2019;17(5):479–505.
  8. Mottet N, Bellmunt J, Bolla M, Briers E, Cumberbatch MG, de Santis M, et al. EAU-ESTRO-SIOG guidelines on prostate cancer. Part 1: Screening, diagnosis, and local treatment with curative intent. *Eur Urol*. 2017;71(4):618–29.
  9. Parker C, Gillessen S, Heidenreich A, Horwich A, Committee EG. Cancer of the prostate: ESMO clinical practice guidelines for diagnosis, treatment and follow-up. *Ann Oncol*. 2015;26 (Suppl 5):v69–77.
  10. Fanti S, Goffin K, Hadaschik BA, Herrmann K, Maurer T, MacLennan S, et al. Consensus statements on PSMA PET/CT response assessment criteria in prostate cancer. *Eur J Nucl Med Mol Imaging*. 2020. <https://doi.org/10.1007/s00259-020-04934-4>.
  11. Crawford ED, Koo PJ, Shore N, Slovin SF, Concepcion RS, Freedland SJ, et al. A clinician’s guide to next generation imaging in patients with advanced prostate cancer (RADAR III). *J Urol*. 2019;201(4):682–92.
  12. Padhani AR, Lecouvet FE, Tunariu N, Koh DM, de Keyzer F, Collins DJ, et al. METastasis reporting and data system for prostate cancer: practical guidelines for acquisition, interpretation, and reporting of whole-body magnetic resonance imaging-based evaluations of multiorgan involvement in advanced prostate cancer. *Eur Urol*. 2017;71(1):81–92.
  13. Mouloupoulos LA, Koutoulidis V. Whole-body MRI of the bone marrow: reporting. *J Magn Reson Imaging*. 2019;49(2):325–7.
  14. Barkhausen J, Quick HH, Lauenstein T, Goyen M, Ruehm SG, Laub G, et al. Whole-body MR imaging in 30 seconds with real-time true FISP and a continuously rolling table platform: feasibility study. *Radiology*. 2001;220(1):252–6.
  15. Lauenstein TC, Freudenberg LS, Goehde SC, Ruehm SG, Goyen M, Bosk S, et al. Whole-body MRI using a rolling table platform for the detection of bone metastases. *Eur Radiol*. 2002;12(8):2091–9.
  16. Hynes JP, Hughes N, Cunningham P, Kavanagh EC, Eustace SJ. Whole-body MRI of bone marrow: a review. *J Magn Reson Imaging*. 2019;50:1687–701.
  17. Li S, Sun F, Jin ZY, Xue HD, Li ML. Whole-body diffusion-weighted imaging: technical improvement and preliminary results. *J Magn Reson Imaging*. 2007;26(4):1139–44.
  18. Gruber B, Froeling M, Leiner T, Klomp DWJ. RF coils: a practical guide for nonphysicists. *J Magn Reson Imaging*. 2018;48:590–604.
  19. Deshmane A, Gulani V, Griswold MA, Seiberlich N. Parallel MR imaging. *J Magn Reson Imaging*. 2012;36(1):55–72.
  20. Dietrich O, Geith T, Reiser MF, Baur-Melnyk A. Diffusion imaging of the vertebral bone marrow. *NMR Biomed*. 2017;30(3):163–70.
  21. Koh DM, Blackledge M, Padhani AR, Takahara T, Kwee TC, Leach MO, et al. Whole-body diffusion-weighted MRI: tips, tricks, and pitfalls. *AJR Am J Roentgenol*. 2012;199(2):252–62.
  22. Pasoglou V, Michoux N, Peeters F, Larbi A, Tombal B, Selleslagh T, et al. Whole-body 3D T1-weighted MR imaging in patients with prostate cancer: feasibility and evaluation in screening for metastatic disease. *Radiology*. 2015;275(1):155–66.
  23. Bernstein MA, Huston J III, Ward HA. Imaging artifacts at 3.0T. *J Magn Reson Imaging*. 2006;24(4):735–46.
  24. Siegel RL, Miller KD, Jemal A. Cancer statistics, 2018. *CA Cancer J Clin*. 2018;68(1):7–30.
  25. Gandaglia G, Abdollah F, Schiffmann J, Trudeau V, Shariat SF, Kim SP, et al. Distribution of metastatic sites in patients with prostate cancer: a population-based analysis. *Prostate*. 2014;74(2):210–6.
  26. Weckermann D, Goppelt M, Dorn R, Wawroschek F, Harzmann R. Incidence of positive pelvic lymph nodes in patients with prostate cancer, a prostate-specific antigen (PSA) level of < or =10 ng/mL and biopsy Gleason score of < or =6, and their influence on PSA progression-free survival after radical prostatectomy. *BJU Int*. 2006;97(6):1173–8.
  27. Halabi S, Kelly WK, Ma H, Zhou H, Solomon NC, Fizazi K, et al. Meta-analysis evaluating the impact of site of metastasis on overall survival in men with castration-resistant prostate cancer. *J Clin Oncol*. 2016;34(14):1652–9.
  28. Bubendorf L, Schopfer A, Wagner U, Sauter G, Moch H, Willi N, et al. Metastatic patterns of prostate cancer: an autopsy study of 1,589 patients. *Hum Pathol*. 2000;31(5):578–83.
  29. Barnes A, Alonzi R, Blackledge M, Charles-Edwards G, Collins DJ, Cook G, et al. UKquantitative WB-DWI technical workgroup: consensus meeting recommendations on optimisation, quality control, processing and analysis of quantitative whole-body diffusion-weighted imaging for cancer. *Br J Radiol*. 2018;91(1081):20170577.
  30. Venkitaraman R, Cook GJ, Dearnaley DP, Parker CC, Khoo V, Eeles R, et al. Whole-body magnetic resonance imaging in the detection of skeletal metastases in patients with prostate cancer. *J Med Imaging Radiat Oncol*. 2009;53(3):241–7.
  31. Robson P. Metastatic spinal cord compression: a rare but important complication of cancer. *Clin Med (Lond)*. 2014;14(5):542–5.
  32. Traill ZC, Talbot D, Golding S, Gleeson FV. Magnetic resonance imaging versus radionuclide scintigraphy in screening for bone metastases. *Clin Radiol*. 1999;54(7):448–51.
  33. Lecouvet FE, Simon M, Tombal B, Jamart J, Vande Berg BC, Simoni P. Whole-body MRI (WB-MRI) versus axial skeleton MRI (AS-MRI) to detect and measure bone metastases in prostate cancer (PCa). *Eur Radiol*. 2010;20(12):2973–82.
  34. Eustace S, Tello R, DeCarvalho V, Carey J, Wroblecka JT, Melhem ER, et al. A comparison of whole-body turboSTIR MR imaging and planar 99mTc-methylene diphosphonate scintigraphy in the examination of patients with suspected skeletal metastases. *AJR Am J Roentgenol*. 1997;169(6):1655–61.
  35. Cumming J, Hacking N, Fairhurst J, Ackery D, Jenkins JD. Distribution of bony metastases in prostatic carcinoma. *Br J Urol*. 1990;66(4):411–4.
  36. Lauenstein TC, Goehde SC, Herborn CU, Treder W, Ruehm SG, Debatin JF, et al. Three-dimensional volumetric interpolated breath-hold MR imaging for whole-body tumor staging in less than 15 minutes: a feasibility study. *AJR Am J Roentgenol*. 2002;179(2):445–9.
  37. Pasoglou V, Larbi A, Collette L, Annet L, Jamar F, Machiels JP, et al. One-step TNM staging of high-risk prostate cancer using magnetic resonance imaging (MRI): toward an upfront simplified “all-in-one” imaging approach? *Prostate*. 2014;74(5):469–77.
  38. Lecouvet FE, Larbi A, Pasoglou V, Omoumi P, Tombal B, Michoux N, et al. MRI for response assessment in metastatic bone disease. *Eur Radiol*. 2013;23(7):1986–97.
  39. Mirowitz SA, Apicella P, Reinus WR, Hammerman AM. MR imaging of bone marrow lesions: relative conspicuousness on T1-weighted, fat-

- suppressed T2-weighted, and STIR images. *AJR Am J Roentgenol.* 1994;162(1):215–21.
40. Filograna L, Magarelli N, Cellini F, Manfreda S, Leone A, Colosimo C, et al. Diffusion weighted imaging (DWI) and apparent diffusion coefficient (ADC) values for detection of malignant vertebral bone marrow lesions. *Eur Rev Med Pharmacol Sci.* 2018;22(3):590–7.
  41. Mateo J, Fizazi K, Gillessen S, Heidenreich A, Perez-Lopez R, Oyen WJG, et al. Managing nonmetastatic castration-resistant prostate cancer. *Eur Urol.* 2019;75(2):285–93.
  42. Pezaro C, Omlin A, Lorente D, Rodrigues DN, Ferraldeschi R, Bianchini D, et al. Visceral disease in castration-resistant prostate cancer. *Eur Urol.* 2014;65(2):270–3.
  43. Kwee TC, Takahara T, Ochiai R, Nievelein RA, Luijten PR. Diffusion-weighted whole-body imaging with background body signal suppression (DWIBS): features and potential applications in oncology. *Eur Radiol.* 2008;18(9):1937–52.
  44. Dixon WT. Simple proton spectroscopic imaging. *Radiology.* 1984;153(1):189–94.
  45. Samji K, Alrashed A, Shabana WM, McInnes MD, Bayram E, Schieda N. Comparison of high-resolution T1W 3D GRE (LAVA) with 2-point Dixon fat/water separation (FLEX) to T1W fast spin echo (FSE) in prostate cancer (PCa). *Clin Imaging.* 2016;40(3):407–13.
  46. Ma J, Costelloe CM, Madewell JE, Hortobagyi GN, Green MC, Cao G, et al. Fast Dixon-based multisequence and multiplanar MRI for whole-body detection of cancer metastases. *J Magn Reson Imaging.* 2009;29(5):1154–62.
  47. Costelloe CM, Kundra V, Ma J, Chasen BA, Rohren EM, Bassett RL Jr, et al. Fast Dixon whole-body MRI for detecting distant cancer metastasis: a preliminary clinical study. *J Magn Reson Imaging.* 2012;35(2):399–408.
  48. Costelloe CM, Madewell JE, Kundra V, Harrell RK, Bassett RL Jr, Ma J. Conspicuity of bone metastases on fast Dixon-based multisequence whole-body MRI: clinical utility per sequence. *Magn Reson Imaging.* 2013;31(5):669–75.
  49. Latifoltojar A, Hall-Craggs M, Rabin N, Popat R, Bainbridge A, Dikaos N, et al. Whole body magnetic resonance imaging in newly diagnosed multiple myeloma: early changes in lesional signal fat fraction predict disease response. *Br J Haematol.* 2017;176(2):222–33.
  50. Bray TJP, Singh S, Latifoltojar A, Rajesparan K, Rahman F, Narayanan P, et al. Diagnostic utility of whole body Dixon MRI in multiple myeloma: a multi-reader study. *PLoS One.* 2017;12(7):e0180562.
  51. Lecouvet FE, Pasoglou V, Van Nieuwenhove S, Van Haver T, de Broqueville Q, Denolin V, et al. Shortening the acquisition time of whole-body MRI: 3D T1 gradient echo Dixon vs fast spin echo for metastatic screening in prostate cancer. *Eur Radiol.* 2020;30(6):3083–93.
  52. Johnston EW, Latifoltojar A, Sidhu HS, Ramachandran N, Sokolska M, Bainbridge A, et al. Multiparametric whole-body 3.0-T MRI in newly diagnosed intermediate- and high-risk prostate cancer: diagnostic accuracy and interobserver agreement for nodal and metastatic staging. *Eur Radiol.* 2019;29(6):3159–69.
  53. Burris NS, Johnson KM, Larson PE, Hope MD, Nagle SK, Behr SC, et al. Detection of small pulmonary nodules with ultrashort echo time sequences in oncology patients by using a PET/MR system. *Radiology.* 2016;278(1):239–46.
  54. Rauscher I, Eiber M, Furst S, Souvatzoglou M, Nekolla SG, Ziegler SI, et al. PET/MR imaging in the detection and characterization of pulmonary lesions: technical and diagnostic evaluation in comparison to PET/CT. *J Nucl Med.* 2014;55(5):724–9.
  55. Afshar-Oromieh A, Haberkorn U, Schlemmer HP, Fenchel M, Eder M, Eisenhut M, et al. Comparison of PET/CT and PET/MRI hybrid systems using a <sup>68</sup>Ga-labelled PSMA ligand for the diagnosis of recurrent prostate cancer: initial experience. *Eur J Nucl Med Mol Imaging.* 2014;41(5):887–97.
  56. Stolzmann P, Veit-Haibach P, Chuck N, Rossi C, Frauenfelder T, Alkadi H, et al. Detection rate, location, and size of pulmonary nodules in trimodality PET/CT-MR: comparison of low-dose CT and Dixon-based MR imaging. *Invest Radiol.* 2013;48(5):241–6.
  57. Messiou C, Giles S, Collins DJ, West S, Davies FE, Morgan GJ, et al. Assessing response of myeloma bone disease with diffusion-weighted MRI. *Br J Radiol.* 2012;85(1020):e1198–203.
  58. Latifoltojar A, Hall-Craggs M, Bainbridge A, Rabin N, Popat R, Rismani A, et al. Whole-body MRI quantitative biomarkers are associated significantly with treatment response in patients with newly diagnosed symptomatic multiple myeloma following bortezomib induction. *Eur Radiol.* 2017;27(12):5325–36.
  59. Maas M, Akkerman EM, Venema HW, Stoker J, Den Heeten GJ. Dixon quantitative chemical shift MRI for bone marrow evaluation in the lumbar spine: a reproducibility study in healthy volunteers. *J Comput Assist Tomogr.* 2001;25(5):691–7.
  60. Karampinos DC, Ruschke S, Dieckmeyer M, Diefenbach M, Franz D, Gersing AS, et al. Quantitative MRI and spectroscopy of bone marrow. *J Magn Reson Imaging.* 2018;47(2):332–53.
  61. Takasu M, Kondo S, Akiyama Y, Takahashi Y, Maeda S, Baba Y, et al. Assessment of early treatment response on MRI in multiple myeloma: comparative study of whole-body diffusion-weighted and lumbar spinal MRI. *PLoS One.* 2020;15(2):e0229607.
  62. Martin J, Arm J, Smart J, Palazzi K, Capp A, Ainsworth P, et al. Spinal multiparametric MRI and DEXA changes over time in men with prostate cancer treated with androgen deprivation therapy: a potential imaging biomarker of treatment toxicity. *Eur Radiol.* 2017;27(3):995–1003.
  63. Perez-Lopez R, Nava Rodrigues D, Figueiredo I, Mateo J, Collins DJ, Koh DM, et al. Multiparametric magnetic resonance imaging of prostate cancer bone disease: correlation with bone biopsy histological and molecular features. *Invest Radiol.* 2018;53(2):96–102.
  64. Maeder Y, Dunet V, Richard R, Becce F, Omoumi P. Bone marrow metastases: T2-weighted Dixon spin-echo fat images can replace T1-weighted spin-echo images. *Radiology.* 2018;286(3):948–59.
  65. Hahn S, Lee YH, Suh JS. Detection of vertebral metastases: a comparison between the modified Dixon turbo spin echo T2 weighted MRI and conventional T1 weighted MRI: a preliminary study in a tertiary centre. *Br J Radiol.* 2018;91(1085):20170782.
  66. Eggers H, Bömert P. Chemical shift encoding-based water-fat separation methods. *J Magn Reson Imaging.* 2014;40(2):251–68.
  67. Kirchgessner T, Acid S, Perlepe V, Lecouvet F, Vande Berg B. Two-point Dixon fat-water swapping artifact: lesion mimicker at musculoskeletal T2-weighted MRI. *Skeletal Radiol.* 2020;49(12):2081–6.
  68. Wu LM, Gu HY, Zheng J, Xu X, Lin LH, Deng X, et al. Diagnostic value of whole-body magnetic resonance imaging for bone metastases: a systematic review and meta-analysis. *J Magn Reson Imaging.* 2011;34(1):128–35.
  69. Balliu E, Boada M, Pelaez I, Vilanova JC, Barceló-Vidal C, Rubio A, et al. Comparative study of whole-body MRI and bone scintigraphy for the detection of bone metastases. *Clin Radiol.* 2010;65(12):989–96.
  70. Johnson KM, Leavitt GD, Kayser HW. Total-body MR imaging in as little as 18 seconds. *Radiology.* 1997;202(1):262–7.
  71. Nakanishi K, Kobayashi M, Nakaguchi K, Kyakuno M, Hashimoto N, Onishi H, et al. Whole-body MRI for detecting metastatic bone tumor: diagnostic value of diffusion-weighted images. *Magn Reson Med Sci.* 2007;6(3):147–55.
  72. Takahara T, Imai Y, Yamashita T, Yasuda S, Nasu S, Van Cauteren M. Diffusion weighted whole body imaging with background body signal suppression (DWIBS): technical improvement using free breathing, STIR and high resolution 3D display. *Radiat Med.* 2004;22(4):275–82.
  73. Padhani AR, Koh DM, Collins DJ. Whole-body diffusion-weighted MR imaging in cancer: current status and research directions. *Radiology.* 2011;261(3):700–18.
  74. Nonomura Y, Yasumoto M, Yoshimura R, Haraguchi K, Ito S, Akashi T, et al. Relationship between bone marrow cellularity and apparent diffusion coefficient. *J Magn Reson Imaging.* 2001;13(5):757–60.

75. Lecouvet FE, Vande Berg BC, Malghem J, Omoumi P, Simoni P. Diffusion-weighted MR imaging: adjunct or alternative to T1-weighted MR imaging for prostate carcinoma bone metastases? *Radiology*. 2009;252(2):624.
76. Herrmann J, Krstin N, Schoennagel BP, Somsakrin M, Derlin T, Busch JD, et al. Age-related distribution of vertebral bone-marrow diffusivity. *Eur J Radiol*. 2012;81(12):4046–9.
77. Herneth AM, Friedrich K, Weidekamm C, Schibany N, Krestan C, Czerny C, et al. Diffusion weighted imaging of bone marrow pathologies. *Eur J Radiol*. 2005;55(1):74–83.
78. Messiou C, Collins DJ, Morgan VA, Desouza NM. Optimising diffusion weighted MRI for imaging metastatic and myeloma bone disease and assessing reproducibility. *Eur Radiol*. 2011;21(8):1713–8.
79. Messiou C, Collins DJ, Morgan VA, Bianchini D, de Bono JS, de Souza NM. Use of apparent diffusion coefficient as a response biomarker in bone: effect of developing sclerosis on quantified values. *Skeletal Radiol*. 2014;43(2):205–8.
80. Eiber M, Beer AJ, Holzapfel K, Tauber R, Ganter C, Weirich G, et al. Preliminary results for characterization of pelvic lymph nodes in patients with prostate cancer by diffusion-weighted MR-imaging. *Invest Radiol*. 2010;45(1):15–23.
81. Beer AJ, Eiber M, Souvatzoglou M, Holzapfel K, Ganter C, Weirich G, et al. Restricted water diffusibility as measured by diffusion-weighted MR imaging and choline uptake in (11)C-choline PET/CT are correlated in pelvic lymph nodes in patients with prostate cancer. *Mol Imaging Biol*. 2011;13(2):352–61.
82. Vag T, Heck MM, Beer AJ, Souvatzoglou M, Weirich G, Holzapfel K, et al. Preoperative lymph node staging in patients with primary prostate cancer: comparison and correlation of quantitative imaging parameters in diffusion-weighted imaging and 11C-choline PET/CT. *Eur Radiol*. 2014;24(8):1821–6.
83. Roy C, Biery G, Matau A, Bazille G, Pasquali R. Value of diffusion-weighted imaging to detect small malignant pelvic lymph nodes at 3 T. *Eur Radiol*. 2010;20(8):1803–11.
84. Thoeny HC, Froehlich JM, Triantafyllou M, Huesler J, Bains LJ, Vermathen P, et al. Metastases in normal-sized pelvic lymph nodes: detection with diffusion-weighted MR imaging. *Radiology*. 2014;273(1):125–35.
85. Jacobs MA, Macura KJ, Zaheer A, Antonarakis ES, Stearns V, Wolff AC, et al. Multiparametric whole-body MRI with diffusion-weighted imaging and ADC mapping for the identification of visceral and osseous metastases from solid tumors. *Acad Radiol*. 2018;25(11):1405–14.
86. Blackledge MD, Leach MO, Collins DJ, Koh DM. Computed diffusion-weighted MR imaging may improve tumor detection. *Radiology*. 2011;261(2):573–81.
87. Blackledge MD, Tunariu N, Orton MR, Padhani AR, Collins DJ, Leach MO, et al. Inter- and intra-observer repeatability of quantitative whole-body, diffusion-weighted imaging (WBDWI) in metastatic bone disease. *PLoS One*. 2016;11(4):e0153840.
88. Souza SP, Szumowski J, Dumoulin CL, Plewes DP, Glover G. SIMA: simultaneous multislice acquisition of MR images by Hadamard-encoded excitation. *J Comput Assist Tomogr*. 1988;12(6):1026–30.
89. Barth M, Breuer F, Koopmans PJ, Norris DG, Poser BA. Simultaneous multislice (SMS) imaging techniques. *Magn Reson Med*. 2016;75(1):63–81.
90. Taron J, Schraml C, Pfannenbergl C, Reimold M, Schwenzer N, Nikolaou K, et al. Simultaneous multislice diffusion-weighted imaging in whole-body positron emission tomography/magnetic resonance imaging for multiparametric examination in oncological patients. *Eur Radiol*. 2018;28(8):3372–83.
91. Buus TW, Sivesgaard K, Jensen AB, Pedersen EM. Simultaneous multislice diffusion-weighted imaging with short tau inversion recovery fat suppression in bone-metastasizing breast cancer. *Eur J Radiol*. 2020;130:109142.
92. Caglic I, Kovac V, Barrett T. Multiparametric MRI—local staging of prostate cancer and beyond. *Radiol Oncol*. 2019;53(2):159–70.
93. Jacobs MA, Wolff AC, Macura KJ, Stearns V, Ouwerkerk R, el Khouli R, et al. Multiparametric and multimodality functional radiological imaging for breast cancer diagnosis and early treatment response assessment. *J Natl Cancer Inst Monogr*. 2015;2015(51):40–6.
94. Panebianco V, De Berardinis E, Barchetti G, Simone G, Leonardo C, Grompone MD, et al. An evaluation of morphological and functional multi-parametric MRI sequences in classifying non-muscle and muscle invasive bladder cancer. *Eur Radiol*. 2017;27(9):3759–66.
95. Sawlani V, Patel MD, Davies N, Flintham R, Wesolowski R, Ughratar I, et al. Multiparametric MRI: practical approach and pictorial review of a useful tool in the evaluation of brain tumours and tumour-like lesions. *Insights Imaging*. 2020;11(1):84.
96. Larbi A, Omoumi P, Pasoglou V, Michoux N, Triqueneaux P, Tombal B, et al. Whole-body MRI to assess bone involvement in prostate cancer and multiple myeloma: comparison of the diagnostic accuracies of the T1, short tau inversion recovery (STIR), and high b-values diffusion-weighted imaging (DWI) sequences. *Eur Radiol*. 2019;29(8):4503–13.
97. Ohlmann-Knafo S, Tarnoki AD, Tarnoki DL, Pickuth DMR. Diagnosis of bone metastases at 1.5T and 3T: can STIR imaging be omitted? *Rofo*. 2015;187(10):924–32.
98. Michoux N, Simoni P, Tombal B, Peeters F, Machiels JP, Lecouvet F. Evaluation of DCE-MRI postprocessing techniques to assess metastatic bone marrow in patients with prostate cancer. *Clin Imaging*. 2012;36(4):308–15.
99. Kayhan A, Yang C, Soylu FN, Lakadamyali H, Sethi I, Karczmar G, et al. Dynamic contrast-enhanced MR imaging findings of bone metastasis in patients with prostate cancer. *World J Radiol*. 2011;3(10):241–5.
100. Bollow M, Knauf W, Korfel A, Taupitz M, Schilling A, Wolf KJ, et al. Initial experience with dynamic MR imaging in evaluation of normal bone marrow versus malignant bone marrow infiltrations in humans. *J Magn Reson Imaging*. 1997;7(1):241–50.
101. Metser U, Chan R, Veit-Haibach P, Ghai S, Tau N. Comparison of MRI sequences in whole-body PET/MRI for staging of patients with high-risk prostate cancer. *AJR Am J Roentgenol*. 2019;212(2):377–81.
102. Messiou C, Hillengass J, Delorme S, Lecouvet FE, Mouloupoulos LA, Collins DJ, et al. Guidelines for acquisition, interpretation, and reporting of whole-body MRI in myeloma: myeloma response assessment and diagnosis system (MY-RADS). *Radiology*. 2019;291(1):5–13.
103. Jager F, Hornegger J. Nonrigid registration of joint histograms for intensity standardization in magnetic resonance imaging. *IEEE Trans Med Imaging*. 2009;28(1):137–50.
104. Belaroussi B, Milles J, Carme S, Zhu YM, Benoit-Cattin H. Intensity non-uniformity correction in MRI: existing methods and their validation. *Med Image Anal*. 2006;10(2):234–46.
105. Zhang H, Xue H, Alto S, Hui L, Kannengiesser S, Berthold K, et al. Integrated shimming improves lesion detection in whole-body diffusion-weighted examinations of patients with plasma disorder at 3 T. *Invest Radiol*. 2016;51(5):297–305.
106. Lin DJ, Johnson PM, Knoll F, Lui YW. Artificial intelligence for MR image reconstruction: an overview for clinicians. *J Magn Reson Imaging*. 2020;1–14. <https://doi.org/10.1002/jmri.27078>.
107. Lavdas I, Glocker B, Rueckert D, Taylor SA, Aboagye EO, Rockall AG. Machine learning in whole-body MRI: experiences and challenges from an applied study using multicentre data. *Clin Radiol*. 2019;74(5):346–56.
108. Lecouvet FE, Geukens D, Stainier A, Jamar F, Jamart J, d’Othée BJ, et al. Magnetic resonance imaging of the axial skeleton for detecting bone metastases in patients with high-risk prostate cancer: diagnostic and cost-effectiveness and comparison with current detection strategies. *J Clin Oncol*. 2007;25(22):3281–7.
109. Luboldt W, Kufer R, Blumstein N, Toussaint TL, Kluge A, Seemann MD, et al. Prostate carcinoma: diffusion-weighted imaging

- as potential alternative to conventional MR and 11C-choline PET/CT for detection of bone metastases. *Radiology*. 2008;249(3):1017–25.
110. Venkitesan R, Cook GJ, Dearnaley DP, Parker CC, Huddart RA, Khoo V, et al. Does magnetic resonance imaging of the spine have a role in the staging of prostate cancer? *Clin Oncol (R Coll Radiol)*. 2009;21(1):39–42.
  111. Gutzzeit A, Doert A, Froehlich JM, Eckhardt BP, Meili A, Scherr P, et al. Comparison of diffusion-weighted whole body MRI and skeletal scintigraphy for the detection of bone metastases in patients with prostate or breast carcinoma. *Skeletal Radiol*. 2010;39(4):333–43.
  112. Mosavi F, Johansson S, Sandberg DT, Turesson I, Sorensen J, Ahlstrom H. Whole-body diffusion-weighted MRI compared with (18)F-NaF PET/CT for detection of bone metastases in patients with high-risk prostate carcinoma. *AJR Am J Roentgenol*. 2012;199(5):1114–20.
  113. Lecouvet FE, El Mouedden J, Collette L, Coche E, Danse E, Jamar F, et al. Can whole-body magnetic resonance imaging with diffusion-weighted imaging replace Tc 99m bone scanning and computed tomography for single-step detection of metastases in patients with high-risk prostate cancer? *Eur Urol*. 2012;62(1):68–75.
  114. Jambor I, Kuisma A, Ramadan S, Huovinen R, Sandell M, Kajander S, et al. Prospective evaluation of planar bone scintigraphy, SPECT, SPECT/CT, 18F-NaF PET/CT and whole body 1.5T MRI, including DWI, for the detection of bone metastases in high risk breast and prostate cancer patients: SKELETA clinical trial. *Acta Oncol*. 2016;55(1):59–67.
  115. Anttinen M, Ettala O, Malaspina S, Jambor I, Sandell M, Kajander S, et al. A prospective comparison of (18)F-prostate-specific membrane antigen-1007 positron emission tomography computed tomography, whole-body 1.5 T magnetic resonance imaging with diffusion-weighted imaging, and single-photon emission computed tomography/computed tomography with traditional imaging in primary distant metastasis staging of prostate cancer (PROSTAGE). *Eur Urol Oncol*. 2020;9311(20):30090–0. <https://doi.org/10.1016/j.euo.2020.06.012>.
  116. Huyse W, Lecouvet F, Castellucci P, Ost P, Lambrecht V, Artigas C, et al. Prospective comparison of F-18 choline PET/CT scan versus axial MRI for detecting bone metastasis in biochemically relapsed prostate cancer patients. *Diagnostics*. 2017;7(4):56.
  117. Eiber M, Rauscher I, Souvatzoglou M, Maurer T, Schwaiger M, Holzapfel K, et al. Prospective head-to-head comparison of (11)C-choline-PET/MR and (11)C-choline-PET/CT for restaging of biochemical recurrent prostate cancer. *Eur J Nucl Med Mol Imaging*. 2017;44(13):2179–88.
  118. Wieder H, Beer AJ, Holzapfel K, Henninger M, Maurer T, Schwarzenboeck S, et al. 11C-choline PET/CT and whole-body MRI including diffusion-weighted imaging for patients with recurrent prostate cancer. *Oncotarget*. 2017;8(39):66516–27.
  119. Zacho HD, Nielsen JB, Afshar-Oromieh A, Haberkorn U, de Souza N, de Paepe K, et al. Prospective comparison of (68)Ga-PSMA PET/CT, (18)F-sodium fluoride PET/CT and diffusion weighted-MRI at for the detection of bone metastases in biochemically recurrent prostate cancer. *Eur J Nucl Med Mol Imaging*. 2018;45(11):1884–97.
  120. Sawicki LM, Kirchner J, Buddensieck C, Antke C, Ullrich T, Schimmöller L, et al. Prospective comparison of whole-body MRI and (68)Ga-PSMA PET/CT for the detection of biochemical recurrence of prostate cancer after radical prostatectomy. *Eur J Nucl Med Mol Imaging*. 2019;46(7):1542–50.
  121. Parker CC, James ND, Brawley CD, Clarke NW, Hoyle AP, Ali A, et al. Radiotherapy to the primary tumour for newly diagnosed, metastatic prostate cancer (STAMPEDE): a randomised controlled phase 3 trial. *Lancet*. 2018;392(10162):2353–66.
  122. Cimino S, Reale G, Castelli T, Favilla V, Giardina R, Russo GI, et al. Comparison between Briganti, Partin and MSKCC tools in predicting positive lymph nodes in prostate cancer: a systematic review and meta-analysis. *Scand J Urol*. 2017;51(5):345–50.
  123. Perera M, Papa N, Roberts M, Williams M, Udovicich C, Vela I, et al. Gallium-68 prostate-specific membrane antigen positron emission tomography in advanced prostate cancer—updated diagnostic utility, sensitivity, specificity, and distribution of prostate-specific membrane antigen-avid lesions: a systematic review and meta-analysis. *Eur Urol*. 2020;77(4):403–17.
  124. Denham JW, Joseph D, Lamb DS, Spry NA, Duchesne G, Matthews J, et al. Short-term androgen suppression and radiotherapy versus intermediate-term androgen suppression and radiotherapy, with or without zoledronic acid, in men with locally advanced prostate cancer (TROG 03.04 RADAR): 10-year results from a randomised, phase 3, factorial trial. *Lancet Oncol*. 2019;20(2):267–81.
  125. Eggener SE, Rumble RB, Armstrong AJ, Morgan TM, Crispino T, Cornford P, et al. Molecular biomarkers in localized prostate cancer: ASCO guideline. *J Clin Oncol*. 2020;38(13):1474–94.
  126. Trabulsi EJ, Rumble RB, Jadvar H, Hope T, Pomper M, Turkbey B, et al. Optimum imaging strategies for advanced prostate cancer: ASCO guideline. *J Clin Oncol*. 2020;38(17):1963–96.
  127. Gillessen S, Attard G, Beer TM, Beltran H, Bjartell A, Bossi A, et al. Management of patients with advanced prostate cancer: report of the Advanced Prostate Cancer Consensus Conference 2019. *Eur Urol*. 2020;77(4):508–47.
  128. Fanti S, Minozzi S, Antoch G, Banks I, Briganti A, Carrio I, et al. Consensus on molecular imaging and theranostics in prostate cancer. *Lancet Oncol*. 2018;19(12):e696–708.
  129. Yang HL, Liu T, Wang XM, Xu Y, Deng SM. Diagnosis of bone metastases: a meta-analysis comparing (1)(8)FDG PET, CT, MRI and bone scintigraphy. *Eur Radiol*. 2011;21(12):2604–17.
  130. Beheshti M, Langsteger W, Fogelman I. Prostate cancer: role of SPECT and PET in imaging bone metastases. *Semin Nucl Med*. 2009;39(6):396–407.
  131. Palmedo H, Marx C, Ebert A, Kreft B, Ko Y, Türler A, et al. Whole-body SPECT/CT for bone scintigraphy: diagnostic value and effect on patient management in oncological patients. *Eur J Nucl Med Mol Imaging*. 2014;41(1):59–67.
  132. Corfield J, Perera M, Bolton D, Lawrentschuk N. (68)Ga-prostate specific membrane antigen (PSMA) positron emission tomography (PET) for primary staging of high-risk prostate cancer: a systematic review. *World J Urol*. 2018;36(4):519–27.
  133. Zacho HD, Nielsen JB, Haberkorn U, Stenholt L, Petersen LJ. (68) Ga-PSMA PET/CT for the detection of bone metastases in prostate cancer: a systematic review of the published literature. *Clin Physiol Funct Imaging*. 2017;38:911–22. <https://doi.org/10.1111/cpf.12480>.
  134. Hofman MS, Lawrentschuk N, Francis RJ, Tang C, Vela I, Thomas P, et al. Prostate-specific membrane antigen PET-CT in patients with high-risk prostate cancer before curative-intent surgery or radiotherapy (proPSMA): a prospective, randomised, multicentre study. *Lancet*. 2020;395(10231):1208–16.
  135. Dyrberg E, Hendel HW, Huynh THV, Klausen TW, Løgager VB, Madsen C, et al. (68)Ga-PSMA-PET/CT in comparison with (18)F-fluoride-PET/CT and whole-body MRI for the detection of bone metastases in patients with prostate cancer: a prospective diagnostic accuracy study. *Eur Radiol*. 2019;29(3):1221–30.
  136. Conde-Moreno AJ, Herrando-Parreño G, Muelas-Soria R, Ferrer-Rebolleda J, Broseta-Torres R, Cozar-Santiago MP, et al. Whole-body diffusion-weighted magnetic resonance imaging (WB-DW-MRI) vs choline-positron emission tomography-computed tomography (choline-PET/CT) for selecting treatments in recurrent prostate cancer. *Clin Transl Oncol*. 2017;19(5):553–61.
  137. Kiss B, Thoeny HC, Studer UE. Current status of lymph node imaging in bladder and prostate cancer. *Urology*. 2016;96:1–7.
  138. Fossati N, Willemsse PM, Van den Broeck T, van den Bergh RCN, Yuan CY, Briers E, et al. The benefits and harms of different extents of lymph node dissection during radical prostatectomy for prostate cancer: a systematic review. *Eur Urol*. 2017;72(1):84–109.
  139. Petersen LJ, Zacho HD. PSMA PET for primary lymph node staging of intermediate and high-risk prostate cancer: an expedited systematic review. *Cancer Imaging*. 2020;20(1):10.

140. Wu H, Xu T, Wang X, Yu YB, Fan ZY, Li DX, et al. Diagnostic performance of (68)gallium labelled prostate-specific membrane antigen positron emission tomography/computed tomography and magnetic resonance imaging for staging the prostate cancer with intermediate or high risk prior to radical prostatectomy: a systematic review and meta-analysis. *World J Mens Health*. 2020;38(2):208–19.
141. Lowrance W, Breau R, Chou R, Chapin BF, Crispino T, Dreice R, et al. *Advanced prostate cancer: AUA/ASTRO/SUO guideline*. American Urological Association; 2020;1(205):14–21.
142. Larbi A, Dallaudiere B, Pasoglou V, Padhani A, Michoux N, Vande Berg BC, et al. Whole body MRI (WB-MRI) assessment of metastatic spread in prostate cancer: therapeutic perspectives on targeted management of oligometastatic disease. *Prostate*. 2016;76(11):1024–33.
143. Phillips R, Shi WY, Deek M, Radwan N, Lim SJ, Antonarakis ES, et al. Outcomes of observation vs stereotactic ablative radiation for oligometastatic prostate cancer: the ORIOLE phase 2 randomized clinical trial. *JAMA Oncol*. 2020;6(5):650–9.
144. Robertson NL, Sala E, Benz M, Landa J, Scardino P, Scher HI, et al. Combined whole body and multiparametric prostate magnetic resonance imaging as a 1-step approach to the simultaneous assessment of local recurrence and metastatic disease after radical prostatectomy. *J Urol*. 2017;198(1):65–70.
145. Eiber M, Holzapfel K, Ganter C, Eppler K, Metz S, Geinitz H, et al. Whole-body MRI including diffusion-weighted imaging (DWI) for patients with recurring prostate cancer: technical feasibility and assessment of lesion conspicuity in DWI. *J Magn Reson Imaging*. 2011;33(5):1160–70.
146. Adeleke S, Latifoltojar A, Sidhu H, Galazi M, Shah TT, Clemente J, et al. Localising occult prostate cancer metastasis with advanced imaging techniques (LOCATE trial): a prospective cohort, observational diagnostic accuracy trial investigating whole-body magnetic resonance imaging in radio-recurrent prostate cancer. *BMC Med Imaging*. 2019;19(1):90.
147. de Wit R, de Bono J, Sternberg CN, Fizazi K, Tombal B, Wülfing C, et al. Cabazitaxel versus abiraterone or enzalutamide in metastatic prostate cancer. *N Engl J Med*. 2019;381(26):2506–18.
148. Schwartz LH, Litiere S, de Vries E, Ford R, Gwyther S, Mandrekar S, et al. RECIST 1.1—update and clarification: from the RECIST committee. *Eur J Cancer*. 2016;62:132–7.
149. Cook GJ, Venkiteraman R, Sohaib AS, Lewington VJ, Chua SC, Huddart RA, et al. The diagnostic utility of the flare phenomenon on bone scintigraphy in staging prostate cancer. *Eur J Nucl Med Mol Imaging*. 2011;38(1):7–13.
150. Scher HI, Morris MJ, Stadler WM, Higano C, Basch E, Fizazi K, et al. Trial design and objectives for castration-resistant prostate cancer: updated recommendations from the prostate cancer clinical trials working group 3. *J Clin Oncol*. 2016;34(12):1402–18.
151. Morris MJ, Autio KA, Basch EM, Danila DC, Larson S, Scher HI. Monitoring the clinical outcomes in advanced prostate cancer: what imaging modalities and other markers are reliable? *Semin Oncol*. 2013;40(3):375–92.
152. Eisenhauer EA, Therasse P, Bogaerts J, Schwartz LH, Sargent D, Ford R, et al. New response evaluation criteria in solid tumours: revised RECIST guideline (version 1.1). *Eur J Cancer*. 2009;45(2):228–47.
153. Lecouvet FE. Whole-body MR imaging: musculoskeletal applications. *Radiology*. 2016;279(2):345–65.
154. Tombal B, Rezazadeh A, Therasse P, Van Cangh PJ, Vande Berg B, Lecouvet FE. Magnetic resonance imaging of the axial skeleton enables objective measurement of tumor response on prostate cancer bone metastases. *Prostate*. 2005;65(2):178–87.
155. Reischauer C, Froehlich JM, Koh DM, Graf N, Padevit C, John H, et al. Bone metastases from prostate cancer: assessing treatment response by using diffusion-weighted imaging and functional diffusion maps—initial observations. *Radiology*. 2010;257(2):523–31.
156. Messiou C, Collins DJ, Giles S, de Bono JS, Bianchini D, de Souza NM. Assessing response in bone metastases in prostate cancer with diffusion weighted MRI. *Eur Radiol*. 2011;21(10):2169–77.
157. Blackledge MD, Collins DJ, Tunariu N, Orton MR, Padhani AR, Leach MO, et al. Assessment of treatment response by total tumor volume and global apparent diffusion coefficient using diffusion-weighted MRI in patients with metastatic bone disease: a feasibility study. *PLoS One*. 2014;9(4):e91779.
158. Perez-Lopez R, Lorente D, Blackledge MD, Collins DJ, Mateo J, Bianchini D, et al. Volume of bone metastasis assessed with whole-body diffusion-weighted imaging is associated with overall survival in metastatic castration-resistant prostate cancer. *Radiology*. 2016;280(1):151–60.
159. Perez-Lopez R, Mateo J, Mossop H, Blackledge MD, Collins DJ, Rata M, et al. Diffusion-weighted imaging as a treatment response biomarker for evaluating bone metastases in prostate cancer: A pilot study. *Radiology*. 2017;283(1):168–77.
160. Yu YS, Li WH, Li MH, Meng X, Kong LI, Yu JM. False-positive diagnosis of disease progression by magnetic resonance imaging for response assessment in prostate cancer with bone metastases: a case report and review of the pitfalls of images in the literature. *Oncol Lett*. 2015;10(6):3585–90.
161. Padhani AR, Koh DM. Diffusion MR imaging for monitoring of treatment response. *Magn Reson Imaging Clin N Am*. 2011;19(1):181–209.
162. Padhani AR, Tunariu N. Metastasis reporting and data system for prostate cancer in practice. *Magn Reson Imaging Clin N Am*. 2018;26(4):527–42.
163. Yoshida S, Takahara T, Ishii C, Arita Y, Waseda Y, Kijima T, et al. METastasis reporting and data system for prostate cancer as a prognostic imaging marker in castration-resistant prostate cancer. *Clin Genitourin Cancer*. 2020;18(4):e391–6.
164. Afshar-Oromieh A, Debus N, Uhrig M, Hope TA, Evans MJ, Holland-Letz T, et al. Impact of long-term androgen deprivation therapy on PSMA ligand PET/CT in patients with castration-sensitive prostate cancer. *Eur J Nucl Med Mol Imaging*. 2018;45(12):2045–54.
165. Emmett L, Yin C, Crumbaker M, Hruby G, Kneebone A, Epstein R, et al. Rapid modulation of PSMA expression by androgen deprivation: serial (68)Ga-PSMA-11 PET in men with hormone-sensitive and castrate-resistant prostate cancer commencing androgen blockade. *J Nucl Med*. 2019;60(7):950–4.
166. Rosar F, Ribbat K, Ries M, Linxweiler J, Bartholomä M, Maus S, et al. Neuron-specific enolase has potential value as a biomarker for [(18)F]FDG/[(68)Ga]Ga-PSMA-11 PET mismatch findings in advanced mCRPC patients. *EJNMMI Res*. 2020;10(1):52.
167. Fendler WP, Eiber M, Beheshti M, Bomanji J, Ceci F, Cho S, et al. (68)Ga-PSMA PET/CT: joint EANM and SNMMI procedure guideline for prostate cancer imaging: version 1.0. *Eur J Nucl Med Mol Imaging*. 2017;44(6):1014–24.
168. Morote J, Celma A, Roche S, de Torres IM, Mast R, Smedey ME, et al. Who benefits from multiparametric magnetic resonance imaging after suspicion of prostate cancer? *Eur Urol Oncol*. 2019;2(6):664–9.
169. Vargas HA, Hotker AM, Goldman DA, Moskowitz CS, Gondo T, Matsumoto K, et al. Updated prostate imaging reporting and data system (PIRADS v2) recommendations for the detection of clinically significant prostate cancer using multiparametric MRI: critical evaluation using whole-mount pathology as standard of reference. *Eur Radiol*. 2016;26(6):1606–12.
170. Alabousi M, Salameh JP, Gusenbauer K, Samoïlov L, Jafri A, Yu H, et al. Biparametric vs multiparametric prostate magnetic resonance imaging for the detection of prostate cancer in treatment-naïve patients: a diagnostic test accuracy systematic review and meta-analysis. *BJU Int*. 2019;124(2):209–20.
171. Hellman S, Weichselbaum RR. Oligometastases. *J Clin Oncol*. 1995;13(1):8–10.
172. Guckenberger M, Lievens Y, Bouma AB, Collette L, Dekker A, de Souza NM, et al. Characterisation and classification of oligometastatic disease: a European Society for Radiotherapy and Oncology and

- European Organisation for Research and Treatment of cancer consensus recommendation. *Lancet Oncol.* 2020;21(1):e18–28.
173. Slaoui A, Albisinni S, Aoun F, Assenmacher G, al Hajj Obeid W, Diamand R, et al. A systematic review of contemporary management of oligometastatic prostate cancer: fighting a challenge or tilting at windmills? *World J Urol.* 2019;37(11):2343–53.
  174. Lecouvet FE, Oprea-Lager DE, Liu Y, Ost P, Bidaut L, Collette L, et al. Use of modern imaging methods to facilitate trials of metastasis-directed therapy for oligometastatic disease in prostate cancer: a consensus recommendation from the EORTC imaging group. *Lancet Oncol.* 2018;19(10):e534–45.
  175. Decaestecker K, De Meerleer G, Ameye F, Fonteyne V, Lambert B, Joniau S, et al. Surveillance or metastasis-directed therapy for oligometastatic prostate cancer recurrence (STOMP): study protocol for a randomized phase II trial. *BMC Cancer.* 2014;14:671.
  176. Hicks RJ, Murphy DG, Williams SG. Seduction by sensitivity: reality, illusion, or delusion? The challenge of assessing outcomes after PSMA imaging selection of patients for treatment. *J Nucl Med.* 2017;58(12):1969–71.
  177. Murphy DG, Sweeney CJ, Tombal B. “Gotta catch ‘em all”, or do we? Pokemet approach to metastatic prostate cancer. *Eur Urol.* 2017;72(1):1–3.
  178. Pasoglou V, Michoux N, Van Damme J, Van Nieuwenhove S, Halut M, Triqueneaux P, et al. Pattern of metastatic deposit in recurrent prostate cancer: a whole-body MRI-based assessment of lesion distribution and effect of primary treatment. *World J Urol.* 2019;37(12):2585–95.
  179. Lee MS, Cho JY, Kim SY, Cheon GJ, Moon MH, OH S, et al. Diagnostic value of integrated PET/MRI for detection and localization of prostate cancer: comparative study of multiparametric MRI and PET/CT. *J Magn Reson Imaging.* 2017;45(2):597–609.
  180. Park H, Wood D, Hussain H, Meyer CR, Shah RB, Johnson TD, et al. Introducing parametric fusion PET/MRI of primary prostate cancer. *J Nucl Med.* 2012;53(4):546–51.
  181. Chen M, Zhang Q, Zhang C, Zhou YH, Zhao X, Fu Y, et al. Comparison of (68)Ga-prostate-specific membrane antigen (PSMA) positron emission tomography/computed tomography (PET/CT) and multiparametric magnetic resonance imaging (MRI) in the evaluation of tumor extension of primary prostate cancer. *Transl Androl Urol.* 2020; 9(2):382–90.
  182. Souvatzoglou M, Eiber M, Takei T, Fürst S, Maurer T, Gaertner F, et al. Comparison of integrated whole-body [11C]choline PET/MR with PET/CT in patients with prostate cancer. *Eur J Nucl Med Mol Imaging.* 2013;40(10):1486–99.
  183. Freitag MT, Radtke JP, Hadaschik BA, Kopp-Schneider A, Eder M, Kopka K, et al. Comparison of hybrid (68)Ga-PSMA PET/MRI and (68)Ga-PSMA PET/CT in the evaluation of lymph node and bone metastases of prostate cancer. *Eur J Nucl Med Mol Imaging.* 2016;43(1):70–83.
  184. Peder EZ, Larson Valentina TMR. Pulse Sequences for PET/MRI. In: Lagaru Andrei HT, Patrick V-H, editors. *PET/MRI in oncology.* Volume 1. 1st ed. Cham: Springer; 2018. p. 27–39.
  185. Mayerhoefer ME, Archibald SJ, Messiou C, Staudenherz A, Berzaczy D, Schöder H. MRI and PET/MRI in hematologic malignancies. *J Magn Reson Imaging.* 2020;51(5):1325–35.
  186. Kinahan PE, Townsend DW, Beyer T, Sashin D. Attenuation correction for a combined 3D PET/CT scanner. *Med Phys.* 1998;25(10):2046–53.
  187. Evangelista L, Zattoni F, Cassarino G, Artioli P, Cecchin D, dal Moro F, et al. PET/MRI in prostate cancer: A systematic review and meta-analysis. *Eur J Nucl Med Mol Imaging.* 2020. <https://doi.org/10.1007/s00259-020-05025-0>.
  188. Guberina N, Hetkamp P, Ruebben H, Fendler W, Grueneisen J, Suntharalingam S, et al. Whole-body integrated [(68)Ga]PSMA-11-PET/MR imaging in patients with recurrent prostate cancer: comparison with whole-body PET/CT as the standard of reference. *Mol Imaging Biol.* 2020;22(3):788–96.